Nanoscale
Advances

REVIEW

View Article Online
View Journal | View Issue

Cite this: *Nanoscale Adv.*, 2022, **4**, 1494

Foldable batteries: from materials to devices

Insu Jeong, †[a] Dong-Yeob Han,†[a] Jongha Hwang,†[b] Woo-Jin Song*[b] and Soojin Park *[a]

Received 26th December 2021
Accepted 3rd February 2022

DOI: 10.1039/d1na00892g

rsc.li/nanoscale-advances

Wearable electronics is a growing field that has important applications in advanced human-integrated systems with high performance and mechanical deformability, especially foldable characteristics. Although foldable electronics such as rollable TVs (LG signature OLED R) or foldable smartphones (Samsung Galaxy Z fold/flip series) have been successfully established in the market, these devices are still powered by rigid and stiff batteries. Therefore, to realize fully wearable devices, it is necessary to develop state-of-the-art foldable batteries with high performance and safety in dynamic deformation states. In this review, we cover the recent progress in developing materials and system designs for foldable batteries. The Materials section is divided into three sections aimed at helping researchers choose suitable materials for their systems. Several foldable battery systems are discussed and the combination of innovative materials and system design that yields successful devices is considered. Furthermore, the basic analysis process of electrochemical and mechanical properties is provided as a guide for researchers interested in the evaluation of foldable battery systems. The current challenges facing the practical application of foldable batteries are briefly discussed. This review will help researchers to understand various aspects (from material preparation to battery configuration) of foldable batteries and provide a brief guideline for evaluating the performance of these batteries.

1. Introduction

Wearable electronics have gained increasing attention over the past few years due to their potential for use in applications such as health care devices, sensors, and implantable devices.[1–4] Wearable electronics should be attachable to human skin or implantable in the human body and hence should be both deformable and soft.[5] Deformation commonly includes bending, twisting, folding, and stretching, but can be simplified to only folding and stretching. A wide range of "folding" processes include all deformations, except for stretching that is governed by a different mechanism and therefore requires further innovative strategies.[6] Hereafter, deformability will refer mainly to foldability (rather than stretchability), and various systems will be discussed in this regard. In recent years, considerable efforts are focused on achieving foldability accompanied by comfort, light weight, and high performance. Foldable displays, represented by rollable TVs (LG signature

---

[a] *Department of Chemistry, Pohang University of Science and Technology, Pohang 37673, South Korea. E-mail: soojin.park@postech.ac.kr*

[b] *Department of Organic Materials Engineering, Chungnam National University, Daejeon 34134, South Korea. E-mail: wjsong@cnu.ac.kr*

† These authors contributed equally to this work.

Insu Jeong is a M.S.-PhD integrated course student in the Department of Chemistry at Pohang University of Science and Technology (POSTECH). He received his B.S. in Chemistry from POSTECH in 2019. His research interest focuses on aqueous lithium-ion batteries.

Dong-Yeob Han is a M.S.-PhD integrated course student in the Department of Chemistry at Pohang University of Science and Technology (POSTECH). He received his B.S. in Chemical Engineering from Ulsan National Institute of Science and Technology (UNIST) in 2019. His research interest focuses on polymer design for high-energy-density Li batteries.

OLED R) or foldable smartphones (Samsung Galaxy Z fold/flip series), have been developed and successfully established in the market. These displays showed that foldability can be achieved even in multilayered structures, and that the realization of next-generation wearable devices has begun. In this regard, batteries, which supply power to a device (including displays), must satisfy the current state-of-the-art foldability requirements while maintaining excellent performance. However, the development remains in an early stage. A significant breakthrough is required for foldable batteries.

Normally, batteries consist of electrodes, a separator, and an electrolyte. However, direct use of the materials comprising these components in foldable batteries is limited by various factors (Fig. 1). Electrodes are commonly manufactured *via* slurry casting on rigid metal current collectors (copper and aluminum). The slurry is composed of active materials mixed with polymeric binders (*e.g.*, polyvinylidene fluoride (PVDF)) and conductive additives, and can be easily delaminated from the collector when external mechanical stimuli are applied. Moreover, electrolytes consisting of organic solvents (*e.g.*, ethylene carbon) and lithium salts (*e.g.*, lithium hexafluorophosphate ($LiPF_6$)) can lead to leakage from packing materials during the deformation process. Solid-state or gel-polymer electrolytes, which can serve as a separator membrane, are considered promising alternatives to their liquid counterparts as the leakage and flammability issue can be avoided. However, even when all components are successfully substituted with suitable materials for foldable batteries, the whole system may exhibit insufficient foldability due to mechanical modulus mismatch of each component under an external stress. Therefore, the entire battery system and each component of the battery must be reinvented in order to satisfy the requirements of high mechanical durability and excellent and stable electrochemical performance for practical applications.

Intrinsically foldable components have been developed for achieving excellent foldability and electrochemical properties. This is especially true for electrodes, where replacement of the alternating rigid metal current collector was considered urgent. For example, carbon materials such as carbon nanotubes, graphene, or carbon cloths can serve as an excellent backbone structure, which is highly conductive and foldable. Unlike the conventional battery systems, the reported systems may sometimes (rather than always) include components (such as binders, current collectors, or separators) for realizing high durability under repeated deformation.[7] Material development and innovative system designs such as patterning,[8] island structures,[9] or kirigami/origami structures[10,11] have been reported as strategies for achieving foldable batteries by decoupling the system into an energy-storage section and a foldable section. The reported systems exhibited high deformability and employed rigid but highly conductive components of conventional batteries.

Several reviews have discussed the materials and battery system designs associated with flexible battery systems.[7,12,13] However, these reviews have focused only on lithium-ion batteries or primarily on materials, and in most cases the definition of flexibility between folding and stretching is ambiguous. A comprehensive review, which considers materials

Jongha Hwang is a M.S.-PhD integrated course student in the Department of Polymer Engineering at Chungnam National University. He received his B.S. in Polymer Engineering in 2015. His research focuses on design and synthesis of polymer materials for energy-storage devices.

Woo-Jin Song received his PhD from the School of Energy and Chemical Engineering at Ulsan National Institute of Science and Technology (UNIST). He spent one year as a postdoctoral researcher at Stanford University. Now he is an assistant professor in the Department of Organic Materials Engineering at Chungnam National University. His research interests include synthesis of polymer materials for energy-storage-devices and design of next-generation batteries such as flexible/stretchable batteries and aqueous zinc-ion batteries.

Soojin Park is a full professor in the Department of Chemistry at POSTECH. He leads the polymer-based energy materials lab for various energy storage applications. Among other honors, he has received the PhD thesis award from The Polymer Society of Korea (2004), the Asia Excellence (The Society of Polymer Science, Japan, 2012), KCS-Wiley Young Chemist Award (2012), Korea Young Scientist Presidential Award (2013), and Researcher Academy Award (The Polymer Society of Korea, 2017). His current research mainly focuses on deformable batteries and design of high capacity anode materials.

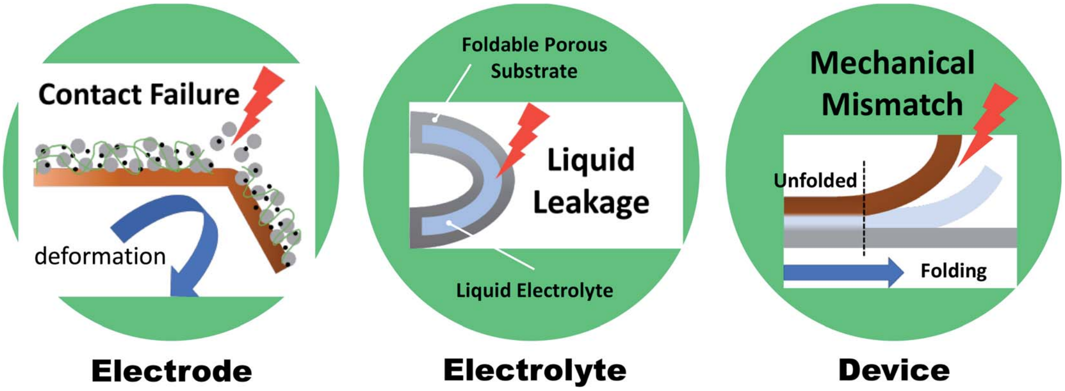

Fig. 1 Hurdles in foldable batteries.

with battery system designs and a wide range of foldable batteries, is therefore still necessary. In this review, we focus mainly on the design strategies of materials and various devices for achieving foldability with practical electrochemical and mechanical performances. First, recent progress in developing materials and system designs for foldable batteries is summarized. The Materials section is further divided into three parts (based on the dimensional nanostructures) in order to help researchers choose suitable materials for their systems. Various foldable battery systems including lithium-ion batteries, air batteries (Zn–air and Li–air), and multi-valent batteries (Zn and Mg) are then introduced and the combination of innovative materials and system designs for achieving successful devices is discussed. In addition, the basic process of electrochemical and mechanical analysis is provided to guide researchers in the evaluation of foldable battery systems. At the end of this review, current challenges facing the practical applications of foldable batteries are briefly covered. This review will help researchers to understand various aspects (from material preparation to battery configuration) of foldable batteries and provide a brief guideline for evaluating the performance of such batteries.

2. Morphologies of materials

A well-designed structure of materials can maintain the original formation in the folding or bending state in foldable batteries and hence the morphologies of materials play a significant role in the flexibility of these batteries.[14–16] Furthermore, the dimensional stability of electrodes is critical to mechanical properties associated with the excellent cohesion and adhesion among active materials, binders, and conducting agents.[17] Even if flexible materials are included in the electrode, selecting unsuitable materials for electrode flexibility can destroy the device in the folding state.[18] Therefore, we should determine the mechanical properties of each electrode component material with various dimensions in order to achieve flexibility of foldable and wearable devices. For the perfect fabrication of foldable batteries, we must consider various materials as current collectors, active materials, binders, and additives, and hence, in this work, we investigate the specific materials according to multiple dimensions for foldable batteries. These materials are mainly divided into three categories in the flexible battery system: one-dimensional (1D), two-dimensional (2D), and three-dimensional (3D).[19–23] Many kinds of 1D, 2D, or 3D materials have been studied with the aim of achieving foldable batteries with high dimensional stability. These include carbon fibers (CFs),[24] carbon cloths (CCs),[25] carbon nanotubes (CNTs),[26] graphene,[27] polymeric materials,[28] metal oxides,[29] transition-metal carbides (TMCs),[30] or metal–organic frameworks (MOFs).[31] The mechanical properties, electrochemical performance, and current applicability of these materials in foldable batteries are discussed in this section.

2.1 One-dimensional materials

1D materials such as CFs, CNTs, and metal wires are considered quite suitable for many applications, owing to their numerous active sites and effective channels that generate short ion diffusion pathways for foldable batteries with excellent mechanical performance.[32–34] These materials can enable the entanglement of active materials, and hence mechanical stability is maintained in the folding state. Therefore, 1D materials, which can be classified as carbon-based materials and metal-based materials, are considered excellent candidates for realizing outstanding performance of foldable batteries.[35,36]

2.1.1 Carbon-based materials. 1D carbon-based materials are generally composed of tube-type structures such as CFs or CNTs, which can provide a large surface area, a high electrical conductivity, an effective ion diffusion pathway, and a network structure with high mechanical stability (commercial CNTs: 1315 $m^2\ g^{-1}$, 10^6–10^7 $S\ m^{-1}$, and 10–150 GPa of tensile strength, respectively).[37–39] Significantly, 1D tube-type materials, which inherently exhibit high flexibility, can yield flexible composites for current collectors, flexible substrates, active materials, and conductive additives.[40–42] An electrospinning method is typically employed for the fabrication of 1D-based composite electrodes. Through $Zn(Ac)_2$-assisted electrospinning, Pan and co-workers fabricated Ge-based anode materials using 1D CFs and CNTs for flexible network materials (FGCZ) (Fig. 2a).[43] Their strategy involved the introduction of CNTs into CFs for high electrical conductivity, the enhancement of mechanical properties, the improvement of electron and ion transport, and the

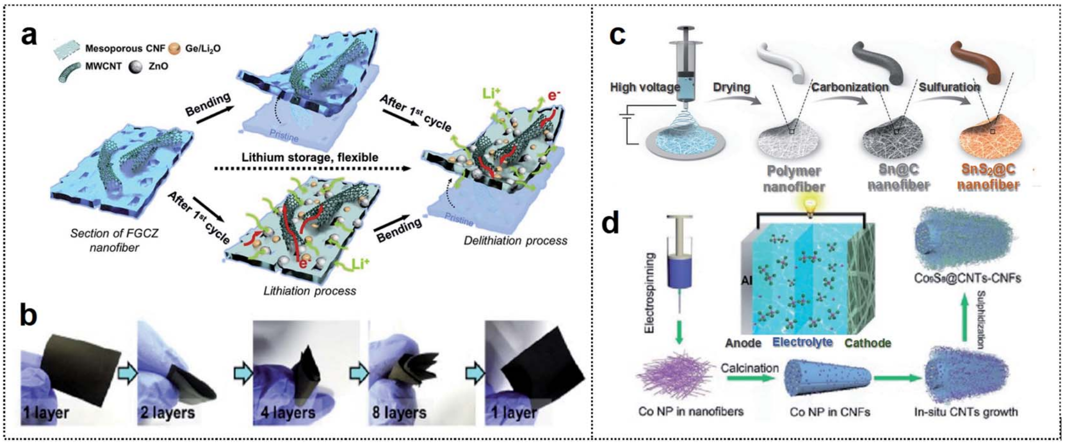

Fig. 2 Carbon-based foldable 1D electrode. (a) Schematic illustration of FGCZ structures and the mechanism for lithium storage. (b) Digital images of the multi-folded FGCZ film and the recovery state of the FGCZ film. Reproduced from ref. 43. Copyright 2019, Elsevier. (c) Schematic illustration of SnS_2@CF by the electrospinning method. Reproduced from ref. 44. Copyright 2021, Royal Society of Chemistry. (d) Schematic illustration of the binder-free and free-standing Co_9S_8@CNT–CNF mats *via* the electrospinning method. Reproduced from ref. 45. Copyright 2018, Wiley-VCH.

suppression of GeO_x volume expansion. FGCZ with CNTs had a high surface area (532.56 *vs.* 246.33 $m^2 g^{-1}$ for reference GCZ) and high mechanical strength (2.1 MPa). This fibrous composite exhibited high mechanical stability by withstanding three-fold folding and recovering its original state without breaking (Fig. 2b). The composite also contributed to the uniform dispersion of GeO_2 nanoparticles, and the full cell with the LCO/CNT cathode and FGCZ anode yielded a high capacity of 847 mA h g^{-1} at a rate of 0.1 A g^{-1}. In addition, a high capacitance retention of 87.5% after 500 cycles, and turned on light-emitting diodes (LEDs) under dynamic folding were observed.

A polymer-based electrospinning method can also be utilized for the fabrication of 1D CF scaffold. Ci and co-workers reported SnS_2-based nitrogen/sulfur (N/S) co-doped CFs as flexible anode materials for foldable K-ion batteries.[44] Polyacrylonitrile (PAN) fiber-derived 1D CF was utilized as the scaffold for depositing Sn particles (Fig. 2c). The carbonized PAN fiber with metal particles could provide a high capacity of 323.9 mA h g^{-1} after 30 cycles (80.8% capacity retention). In addition, the fiber enabled operation of 27 LEDs, which remained in operation in 1-fold (180° deformation) and 2-fold states in the SnS_2@C anode-based K ion battery.

1D carbon-based materials can also be used as cathode materials in foldable batteries. Wang and co-workers used an electrospinning method to design a binder-free and free-standing CF film with cobalt sulfide encapsulated CNTs (Co_9S_8@CNT–CNF) as a cathode electrode in flexible Al ion batteries (Fig. 2d).[45] 1D CNTs and CNFs could provide entanglement with a porous network of high surface area (115.1 $m^2 g^{-1}$), and Co_9S_8 particles were well distributed among the CNTs. Consequently, the Co_9S_8@CNT–CNF-based Al ion battery exhibited outstanding cycle stability (87 mA h g^{-1} at 1 A g^{-1} and 90% coulombic efficiency after 6000 cycles) and powered LEDs in the deformation state. 1D carbon-based materials can provide good mechanical properties with high flexibility and good adhesion among flexible substrates, active materials, and conductive additives. However, these materials are sometimes easily aggregated, leading to self-entanglement due to strong π–π interactions, and limited flexibility of the electrodes.[46,47] Therefore, the appropriate utilization and combination of 1D carbon-based materials are crucial for various foldable batteries.

2.1.2 **Metal-based materials.**

Owing to their high flexibility, easy processability, efficient charge transfer, and high electrical conductivity, 1D metal-based materials exhibit significant potential for use in energy-storage-devices.[48–50] This is especially true for metal wires with significantly higher electrical conductivity than 1D carbon-based materials (CNT & CF: 1 × 10^6–10^7 *vs.* Cu & Ag: 6–7 × 10^7 S m^{-1}).[51] Polymeric binders can reduce the electrical conductivity of metal-based materials and lead to limited flexibility of the electrode. Hence, to utilize 1D metal-based materials for foldable batteries, we must consider the mechanical cohesion among active materials for cathodes and anodes, polymeric binders such as polyvinylidene fluoride (PVDF) and polyacrylic acid (PAA), and conductive agents.[52–54] Therefore, optimized architectures of additives and active materials achieved through innovative fabrication methods are needed for foldable batteries. Park and co-workers obtained current collector-free and binder-free nanowire-around-microfiber (NW@MF) architectures with high flexibility and capacity scalability using the ultrasonic spray-coating method for flexible or wearable devices (Fig. 3a).[55] They designed two kinds of Ag nanowire (NW) wound polyethylene terephthalates (PETs) using the ultrasonic spray method. The AgNWs developed strongly interlocking joints with uniform dispersion, but the CNTs were slightly aggregated on the substrate because Ag was more ductile than the CNTs and the CNT–CNT interaction was stronger than the CNT–PET substrate interaction. Therefore, the 1D network of NW@MFs provided the mechanical stability in the deformation state, as confirmed by scanning electron microscopy images of the folding edge (see Fig. 3b). The novel

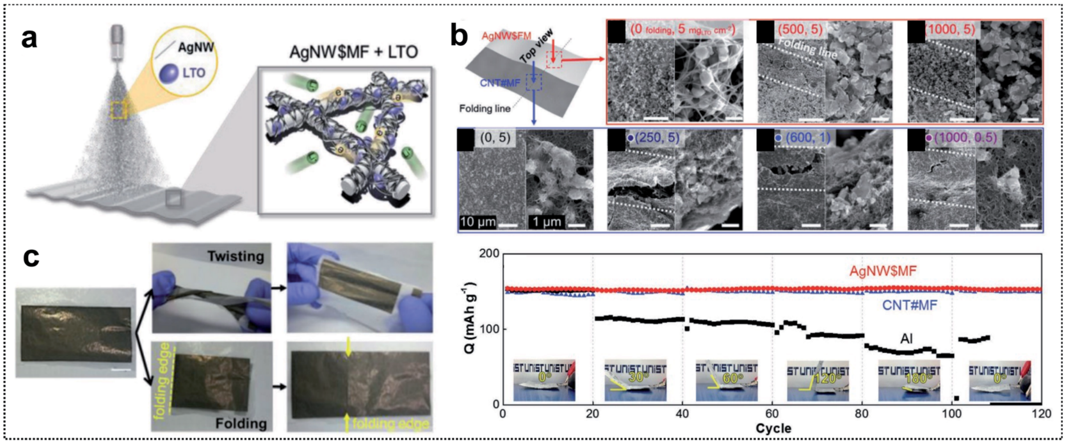

Fig. 3 Metal-based foldable 1D electrode. (a) Schematic illustration of LTO-loaded AgNW$MF. (b) SEM images of the foldable electrode. (up) Top-view images of LTO-loaded AgNW$MF: before folding, after 500 folding cycles, and after 1000 folding cycles. (Down) Top-view images of LTO-loaded CNT#MF: in 5 mg_{LTO} cm^{-2} before folding, in 5 mg_{LTO} cm^{-2} after 250 folding cycles, in 1 mg_{LTO} cm^{-2} after 600 folding cycles and in 0.5 mg_{LTO} cm^{-2} after 1000 folding cycles. (c) Digital images of LTO-loaded AgNW$MF after twisting and folding. (d) Capacity retention of folded cells at different angles at 1C. Reproduced from ref. 55. Copyright 2018, Wiley-VCH.

electrode architecture design yielded high capacity at a high mass loading (150 mA h g^{-1} at 5 mg cm^{-2}) without structural deformation or capacity loss after repeated crumpling and folding (Fig. 3c and d). As a result, the performance of the active material (lithium titanate oxide-LTO)-loaded flexible electrode was the same as that of the unfolded electrode (150 mA h g^{-1}). In addition, the areal capacity of this electrode was four times higher than that of the unfolded electrode (3.2 *vs.* 0.8 mA h cm^{-2} at 1C after 1000 cycles). These strategies indicate that the well-designed 1D-based materials of flexible electrodes can be applied to foldable batteries. Most importantly, in 1D-based materials, we can utilize the effective 1D channels for realizing short ion diffusion pathways and outstanding adhesion properties that yield strong entanglements of the active materials, conducting agents, and binders for foldable batteries.

2.2 Two-dimensional materials

The second category of materials is 2D-based materials, composed of flexible sheet-type components such as graphene and TMC (MXene). Generally, 2D crystalline sheets are composed of atomically thin layers with intralayer covalent bonding and interlayer van der Waals bonding,[56,57] which can provide outstanding mechanical properties and high electrical conductivity for foldable batteries.[58–60] These materials lack dangling surface bonds and exhibit excellent electrochemical stability.[61–63] Moreover, 2D sheet-type materials are suitable for flat large-area nanomanufacturing technologies that generate foldable devices.

2.2.1 Carbon-based materials.

Carbon-based 2D materials are generally classified as graphene-based materials. Graphene has been widely studied for flexible electrode materials due to its outstanding properties such as high mechanical properties (130 GPa), large surface area (2630 m^2) for many reactive sites, and high electrical conductivity (80×10^{-6} S m^{-1}).[64,65] The synthesis strategies are normally categorized into three methods, namely (i) mechanical exfoliation of graphene from graphite using the scotch-tape method[66] or liquid-phase exfoliation.[67] However, this physical method is costly and unsuitable for mass-production of practical devices. (ii) Chemical vapor deposition,[68] which is amenable to mass production. However, the transfer steps generate many defects in graphene and the process is therefore quite costly.[69] (iii) Chemical exfoliation of GO.[70,71] GO is composed of numerous oxygen-containing functional groups such as hydroxyl groups (–OH) and carbonyl groups (–COOH, –COH, –C–O–C–).[72,73] The chemical exfoliation method has been widely reported for fabricating composites with other active materials because this process is mass-producible, cost-efficient, and has good processability. For the foldable electrodes, reduction of the contact resistance among the current collectors, active materials, and additives is crucial for high flexibility. Geng and co-workers obtained hybrid composites of titania and chemically exfoliated GO sheets *via* the wet-spinning method (Fig. 4a).[74] This method yielded GO and titania well-stacked in a row with the configuration of a 2D composite (Fig. 4b). The structure provided a high mechanical strength (150–160 MPa) and maintained the electrical conductivity in the bending state (initial: 601 Ω, bending 60, 90, and 120°: 601, 608, and 609 Ω, respectively). This retention resulted from the fact that the material acted as both a charge collector and flexible component due to the strong sheet-to-sheet interaction resulting from partial restoration of π–π conjugations. The full cell with rGO-based titania/$LiMn_2O_4$ resulted in a high capacitance retention (80% (100 mA h g^{-1}) capacity retention after 100 cycles) and powered red LEDs that remained unchanged in the deformation state. Xu and co-workers fabricated flexible and free-standing composites (similar to this foldable electrode) using rGO and poly(3,4-ethylene-dioxythiophene):poly(styrene sulfonate) (SGP), as shown in Fig. 4c.[75] In this case, GO provided a highly conductive pathway for fast charge transportation. The residual oxygen-containing

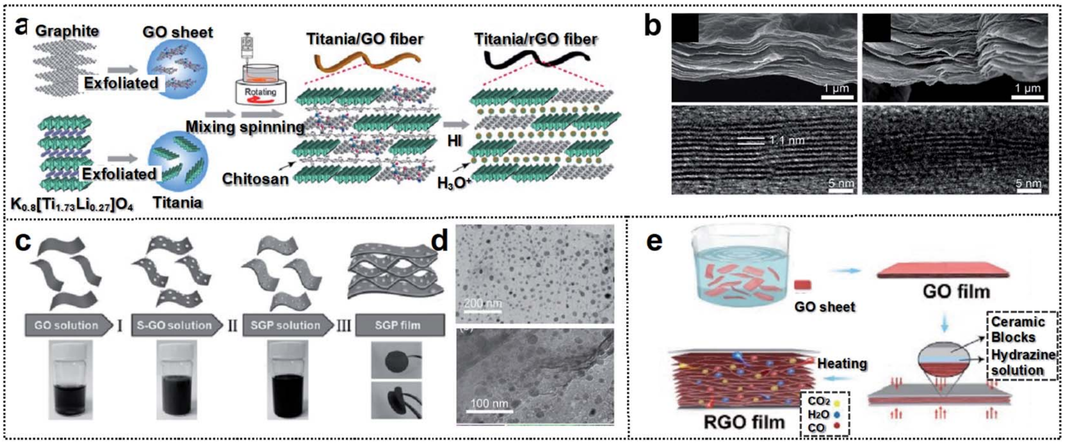

Fig. 4 Carbon-based foldable 2D electrode. (a) Schematic illustration of the fabrication process for the hybrid fiber of titania/rGO (b) SEM (upper panel) and HRTEM (lower panel) images for (left) as-spun dry titania/GO fiber and (right) HI-reduced titania/rGO fiber. Reproduced from ref. 74. Copyright 2017, American Chemical Society. (c) Schematic illustration of the fabrication process of SGP cathodes. (d) TEM images of (up) nano-S grown on GO, and (down) SGP. Reproduced from ref. 75. Copyright 2017, Wiley-VCH. (e) Schematic illustration of the fabrication process of the ultraflexible and porous graphene film. Reproduced from ref. 76. Copyright 2018, Wiley-VCH.

functional groups of GO could enhance the chemical interaction with active materials (Fig. 4d). This compact layered SGP cathode exhibited high capacity (1584 mA h g^{-1} at 0.1C and 701 mA h g^{-1} at 4C) and outstanding cycle stability (80% capacity retention after 500 cycles at 1 g cm^{-3}). Furthermore, the cathode imparted high volumetric energy-storage ability to the Li–sulfur battery system. Therefore, SGP electrodes based on a soft-packed Li–S battery exhibited a volumetric capacity of 1432 A h L^{-1} and turned-on LEDs in the folded state, indicating that rGO could also be utilized as flexible scaffolds for foldable energy-storage-devices.

Yu and co-workers reported a solid-state foldable supercapacitor.[76] They engineered the micro-void distribution of rGO films through a leavening-accompanied reduction treatment of GO films with the spillage of gaseous species such as water and carbon dioxide. This treatment expanded the graphene layers, thereby yielding a porous structure with micro-voids (Fig. 4e). The micro-voids could improve the foldability of the rGO foam structure because the porous films could prevent stress localization and structural breaks at the folding site (no crack formation after 2000 folding cycles). The rGO-based supercapacitor with micro-voids resulted in almost 100% capacitance retention at 5 mV s^{-1} after 2000 cycles of single or double folding (capacitance: 221.6 mF cm^{-2} and energy density: 30.8 μW h cm^{-2}). These studies indicate that the structural engineering of 2D graphene is crucial for the design of foldable storage devices.

2.2.2 MXenes.

MXenes, 2D TMC materials (M_4X_3, M_3X_2, or M_2X), are characterized by high electrical conductivity (2.4×10^{-5} S m^{-1})[77] and outstanding mechanical properties (Young's modulus: 0.33 TPa),[78] and are hence quite desirable for use in energy-storage-devices. Like graphene, the sheet-type MXene is self-assembled into flexible films for foldable electrodes, utilized as an excellent substrate for fabricating composites with other materials such as carbon-based materials,[79] metal-based materials,[80] and conductive polymers.[81] Shen and co-workers designed a MXene-coated textile fabric electrode (MF) with a layer-by-layer structure for Li–S batteries (Fig. 5a).[82] The flexible electrode was composed of a common fabric (CF) as the cost-efficient scaffold for flexibility and MXene nanosheets for fast electron transfer and ion transport channels. For the uniform deposition of MXene on a fabric support, a wet etching process involving hydrochloric acid (HCl) and lithium fluoride (LiF) was employed for the conversion of MXene from the MAX phase. The Li_2S deposition capacity of the MXene-based electrode was considerably higher than that of the CF electrode only (266 mA h g^{-1} *vs.* 189 mA h g^{-1}) due to the rapid transformation of Li_2S induced by the rapid redox kinetics of MF. In addition, MF in the three-electrode system yielded higher capacity retention (73.7% and 44.6% after 1000 cycles) than that of CC (13.8% after 500 cycles). Therefore, the MXene-coated electrode played a crucial role in the high-performance Li–S batteries. This foldable battery demonstrated high performance with excellent capacity retention (674 mA h g^{-1} at 1C after 1000 cycles) and 30 LED operation ability (Fig. 5b).

MXenes can also be used to fabricate composites with other 2D materials (such as graphene) to extend structural advantages of the material. Chen and co-workers used an MXene to fabricate an aerogel with 2D graphene (MGA) for a foldable electrode (Fig. 5c).[83] The resulting MXene/rGO composites provided a large surface area for the dense deposition of active materials. Their integrating strategy provided mechanical strength and a large electrode/electrolyte contact area for high flexibility. Furthermore, the fluorine termination of MXene could inhibit the dendritic growth of Zn during the charge/discharge process, thereby promoting long-term stability. Therefore, the MGA-based electrode exhibited a high coulombic efficiency of 99.67% at a high current density of 10 mA cm^{-2} after 600 cycles. This electrode achieved a lower overpotential (88 *vs.* 33 mV at 60 cycles) than that of commercial Cu foil. The flexible MGA-based Zn-ion batteries with a $LiMn_2O_4$ cathode exhibited excellent deformability without the loss of active materials during the

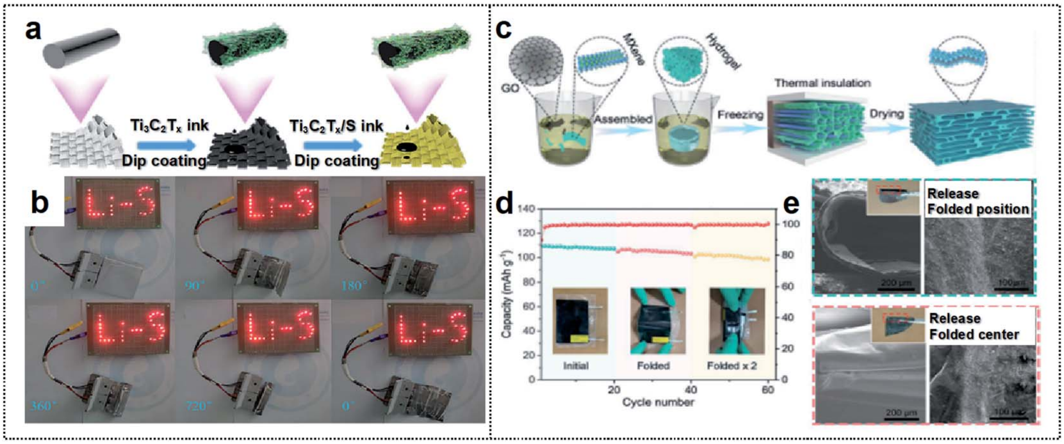

Fig. 5 MXene-based foldable 2D electrode. (a) Schematic illustration of the fabrication process of the MF@$Ti_3C_2T_x$/S cathode. (b) A "Li–S" shaped string of light contains 30 LEDs lit by MF@$Ti_3C_2T_x$/S50 electrode soft-packaged Li–S batteries at different bending angles. Reproduced from ref. 82. Copyright 2021, Royal Society of Chemistry. (c) Schematic illustration of the fabrication process of the MGA material. (d) Cycling performance of the LMO//MGA@Zn pouch cells at various folding times. (e) SEM images of the MGA sample after folding (left) and releasing (right) once (up) and twice (down). The inset images indicate the optical pictures of the MGA sample after folding once (up) and twice (down), respectively. Reproduced from ref. 83. Copyright 2021, Wiley-VCH.

charge/discharge process and a high capacity retention of over 91% after folding cycles (Fig. 5d and e). As a result, the construction of 2D-based materials has a high potential, owing to the excellent mechanical properties and high electrical conductivity achievable for foldable batteries.

2.3 Three-dimensional materials

Regarding foldable devices, 3D-based materials with pores can also be candidates, owing to available mechanical movement of internal space occurring in the free volume and high ion-absorption area from the electrolyte in the deformation state.[84,85] Two fabrication strategies are typically used to construct 3D porous materials: (i) the utilization of 3D precursors such as carbon cloth,[86] carbon aerogel,[87] and metal mesh.[88] (ii) The combination of 1D and 2D materials.[89,90] In the case of 3D substrates, an intrinsically strong and porous network structure can provide mechanical stability to the electrodes and excellent adhesion of active materials, binders, and additives without spalling in the deformation state. Xue and co-workers reported the fabrication process of Ag nanoparticle-deposited 3D carbon cloth obtained *via* the inkjet printing method (Fig. 6a).[91] This method is a cost-efficient process that allows direct deposition on the 3D carbon support for uniform and dense deposition of Ag nanoparticles (Fig. 6b). The results suggested that a heterometallic seed-mediated method prevented dendrite growth of Zn into a 3D substrate *via* the inkjet

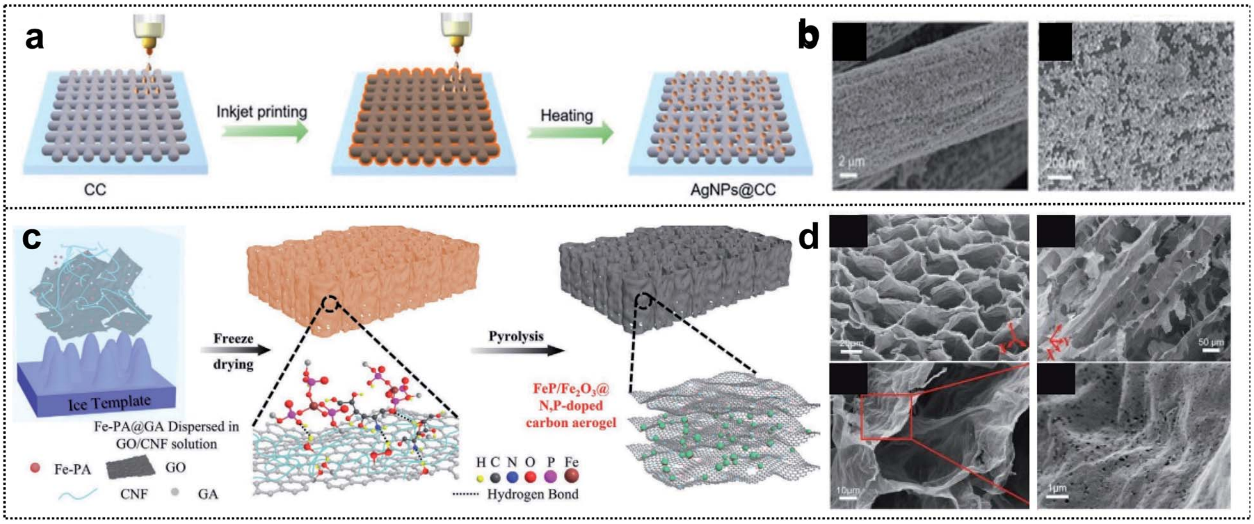

Fig. 6 Foldable 3D electrode. (a) Schematic illustration of the fabrication process of AgNPs@CC. (b) SEM images of AgNPs@CC scaffolds. Reproduced from ref. 91. Copyright 2021, Wiley-VCH. (c) Schematic illustration of the fabrication process of FeP/Fe_2O_3@NPCA. (d) SEM images of FeP/Fe_2O_3@NPCA at different magnifications. Reproduced from ref. 92. Copyright 2020, Wiley-VCH.

printing method, as confirmed through *in situ* optical microscopy during the Zn-plating process of AgNPs@CC scaffolds. The full cell with AgNPs@CC/Zn exhibited a high capacity of 282 mA h g^{-1} at 0.5 A g^{-1}. Correspondingly, foldable batteries with cycling stability (1200 cycles of capacitance retention at 5.0 A g^{-1}) and high capacity at different deformations (~95% of capacity retention in flat, bent, fold, and flat states) were obtained.

Compared with the utilization of 3D precursors, the construction of 1D and 2D composites includes chemical bonding such as covalent bonding among the functional groups of 1D and 2D materials. This has structural advantages for foldable devices due to good accessibility of the electrolyte and the mechanical strength of the 3D network entanglement. Lu and co-workers designed a 3D honeycomb-like carbon aerogel with an FeP/Fe_2O_3@N/P-doped carbon aerogel by utilizing 2D GO and 1D cellulose nanofibrils (CNFs) for foldable cathode materials (Fig. 6c).[92] The strategy exploited the good dispersibility of GO and flexible CNF building blocks in water for excellent mechanical properties, and 1D CNFs prevented the stacking of reduced GO sheets, thereby resulting in a porous structure (Fig. 6d). This carbon aerogel provided outstanding mechanical stability during bending and compression and contributed to efficient electrolyte diffusion and ionic conductivity. The low energy gap of the FeP/Fe_2O_3@N/P-doped carbon aerogel as the electrochemical catalyst for Zn–air batteries was considerably better than those of other catalysts (0.79 *vs.* 0.93 V for FeN_x–C) and even similar to that of commercial noble catalysts (0.73 V). Zn–air batteries with the FeP/Fe_2O_3@N/P-doped carbon aerogel exhibited a high capacity of 676 mA h g^{-1} and an energy density of 517 W h kg^{-1}. Moreover, in the bending state, the assembled foldable battery exhibited high stability with the operation of 12 yellow LEDs. We summarize the advantages of each dimension of materials for foldable batteries. 1D materials guarantee short ion diffusion pathways and outstanding adhesion properties. 2D materials have outstanding mechanical properties and high electrical conductivity. Lastly, 3D materials have both the internal space of free volume and high ion-absorption area in the mechanical deformation state. These material strategies for 1D, 2D, and 3D composites provide inspiration for the development of foldable electrode materials and the practical application of foldable batteries.

2.4 Structural design

Structure design represents a new method for achieving system-level-integration of energy-storage-devices without changing the dimension of materials; this method is compatible with the standard manufacturing processes and is cost effective.[22,93–97] The design of a foldable energy-storage device begins with decoupling of the energy-storage parts (rigid parts) from the flexibility providing parts (soft parts). Furthermore, an appropriate balance between the two sets of parts is necessary for realizing high-performance foldable batteries with stable electrochemical properties. The inspiration (such as calligraphy,[98] folding beds,[99] accordions,[100] spines,[101] and joints[102]) for the structural design of the foldable energy-storage-devices arises mainly from our daily lives. Recently, inspired by the structure of the human spine, Yang and co-workers fabricated a spine-like battery with a high energy density. The schematic presented in Fig. 7a shows the configuration of the battery, which consists of hard components (energy storage) and soft components (flexibility providers) corresponding to the vertebrae and marrow, respectively. The conventional anode, separator, cathode, and polyethylene supporting film were stacked and cut into a long strip with multiple branches. Afterward, the strips, which were wrapped around the backbone, formed thick stacks for high energy density, and unwound parts between the strips provided excellent flexibility to the whole device. The cycling performance was determined in both the flat state and bent state of the spine-like battery (Fig. 7b). Capacity retentions of 99.4% after 20 cycles in the flexed state and 99.4% after 10 cycles in the twisted state (95.6% capacity retention after 50 cycles in the flat state) were observed. This suggested that, owing to the unique structural design of the battery, the deformations had no effect on the cycling performance of the battery. Moreover, during a dynamic mechanical load experiment, the spine-like battery was charged/discharged during repetitive deformations (Fig. 7c). In the dynamic flexed state at 0.5C, the specific discharge capacity decreased in the initial cycles of bending (3.8 mA h g^{-1} from cycles 6–10), but remained steady from the 10th cycle (125.7 mA h g^{-1}) to the 15th cycle (124.6 mA h g^{-1}).

Further developments in structural design included a zigzag-like foldable battery that was fabricated by Yang and co-workers a year after the spine-like battery was developed.[103] The zigzag battery, with excellent foldability and high energy density, was composed of a conventional graphite anode/separator/lithium cobalt oxide cathode with its metal current collectors (Cu and Al foil) and tape. As shown in Fig. 7d, the division segments that act as future folding joints (soft parts) were protected by the thin tape for future deformation. This tape occupied <4% of the area and had little effect on the energy density (<0.5%). Based on the finite element calculation results of the mechanical foldability and durability, Yang *et al.* optimized the structural design for excellent flexibility while maintaining the electrochemical performance of the cell. Fig. 7e shows the selected gap-less structure (zigzag) that can be folded by 180° and become self-compacted, and the smallest bending diameter (d_0) for the fixed length of folding joints compared with that of other structural designs. Regarding the usefulness of thin tape, they showed the strain contours of electrode multilayers at folding joints with and without protective thin tapes in 180° folding states (Fig. 7f). The results revealed that 0.5% and 5.5% of the shear strain were borne by the metal foil in the electrode with and without the protective tape, respectively. Thus, the role of the tape, which covers both sides of the folding joints, in enhancing the mechanical durability of the foldable battery during the deformation was verified.

Zhi and co-workers, inspired by the human joints that can accommodate large deformation, fabricated a foldable lithium-ion battery that is similar to the joints that enable bending, twisting, and even folding. Fig. 7g shows the stack of an anode

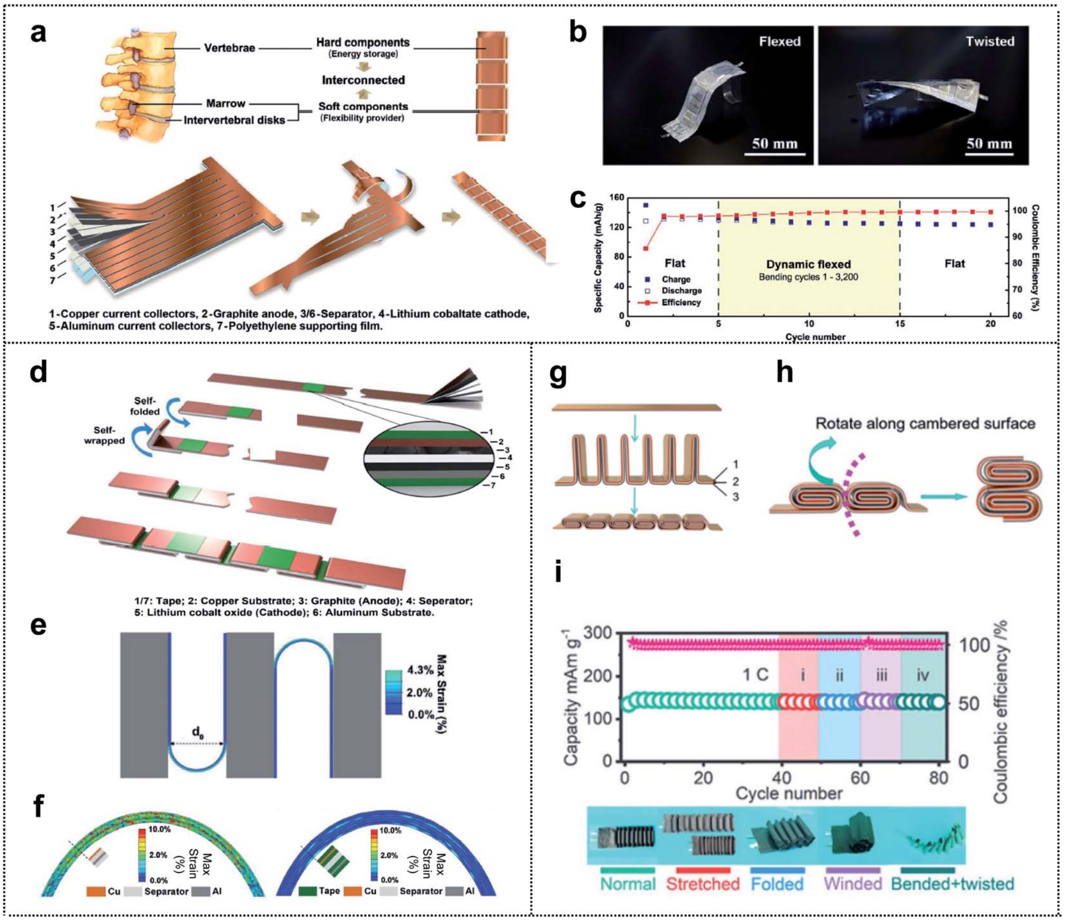

Fig. 7 Structure design. (a) The schematic of the structure and the fabrication process of a spine-like battery. (b) Optical images of the spine battery in the flexed and twisted states. (c) The cycling performance of a spine-like battery in different configurations by a repetitive mechanical load test. Reproduced from ref. 101. Copyright 2018, Wiley-VCH. (d) Fabrication process of a zigzag-like foldable battery. (e) Folding deformation of a zigzag-like battery structure with a bending diameter of 3 mm where the tape length is half of the stack length. (f) Strain contours of electrode multilayers at folding joints without (left) and with (right) protective tapes. Reproduced from ref. 103. Copyright 2019, Wiley-VCH. (g) The schematic of the structure and fabrication process of the flexible batteries, where 1, 2 and 3 correspond to the anode, separator, and cathode, respectively. (h) The folding schematic of the battery with cubic units. (i) Charge/discharge cycling test of the cell with cylindrical units in different configurations at 1C. Reproduced from ref. 102. Copyright 2021, Royal Society of Chemistry.

(1), separator (2), and cathode (3) that is divided into interconnected segments, with each segment folded in half (rigid parts). The two rigid stacks are connected by a junction (soft parts), which serves as the flexibility-providing ligament. Therefore, the designed units (here, cubic units) move along the cambered surface of the thick stack during bending and the additional space between the rigid parts is unnecessary and may be advantageous in terms of increasing energy density (Fig. 7h). They also proposed three types of units, namely triangular prism-shaped, cubic, and cylindrical units. Among batteries consisting of these units, the foldable battery with cylindrical units can bear more severe deformations due to the characteristics of a circle, as confirmed by finite element analysis. To evaluate the electrochemical performance of the designed foldable batteries, the batteries were tested at 1C with various configurations including normal, stretched, folded, wound, bent, and twisted (Fig. 7i). No significant capacity fading for the cells was observed, even under severe mechanical deformation conditions, thereby confirming the well-designed structure of the foldable lithium-ion batteries (LIBs).

3. Devices

3.1 Li-ion batteries

Lithium-ion batteries are considered one of the most promising energy-storage systems for next-generation wearable devices as they have current state-of-the art electrochemical properties such as high energy density and working voltage, and excellent cycle life.[104] Foldable lithium-ion batteries (FLIBs) exhibit excellent mechanical durability and the aforementioned electrochemical characteristics even under repeated deformation. FLIBs can be realized by using foldable electrodes[94,105–107] and electrolytes[108–110] or introducing innovative structural designs.[93]

Recently, Lu and co-workers obtained FLIBs by introducing carbon coated ion exchange synthesized nickel oxide nanosheet arrays into carbon cloth (C@IENiO-CC) as a foldable electrode.

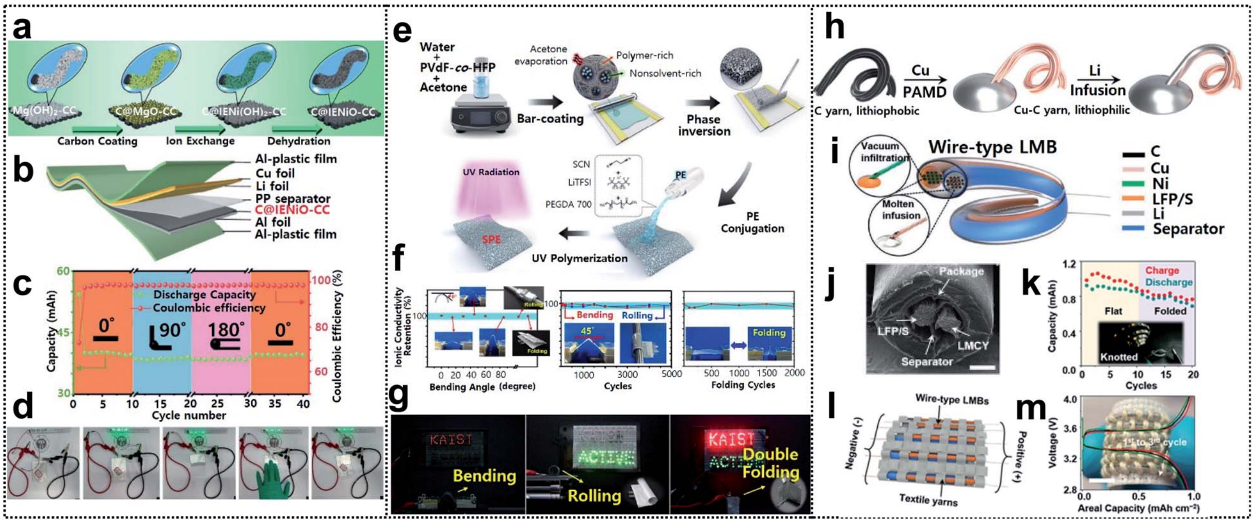

Fig. 8 Foldable lithium-ion batteries. (a) Schematic illustration of fabrication of carbon-coated IE-synthesized NiO nanosheet arrays on CC(C@IENiO-CC), (b) a pouch cell structure based on C@IENiO-CC, (c) cycling performance of the cell in bending states and (d) optical images of the cell lighting up LED bulbs in flat and bended states. Reproduced from ref. 107. Copyright 2021, Wiley-VCH. (e) Schematic procedure for preparing porous PVDF-*co*-HFP intertwined SPE, (f) ionic conductivity under several deformation processes and (g) optical images of LEDs lighted by LFP/40-INSPE 1 : 2/Li with bending, rolling, and double-folding. Reproduced from ref. 109. Copyright 2020, American Chemical Society. (h) Fabrication process of a lithium–metal composite yarn (LMCY), (i) structural design of the wire-type lithium–metal batteries (LMBs), (j) sectional SEM image of the as-fabricated wire-type LFP||LMCY battery, (k) capacity retention of the battery in flat and folded states, and inset shows the optical image of powered LEDs by the knotted batteries, (l) schematic image of the battery textile and (m) voltage profiles of the battery textile, the inset shows the optical image of the as-fabricated battery textile. Reproduced from ref. 111. Copyright 2021, Wiley-VCH.

The electrode can be fabricated through a sequential process – carbon coating, ion exchange, and dehydration, as shown in Fig. 8a. This process allows the electrode to avoid the reduction issue of transition-metal oxides during the high-temperature formation step of carbon coating and preserve the nanostructure of the starting template, such as interwoven $Mg(OH)_2$ nanosheets. FLIBs were assembled into a pouch cell (see Fig. 8b). The cell maintained excellent cycling performance in different bending states (0°, 90°, and 180° followed by returning to 0°) at a current density of 0.25 mA cm^{-2} (Fig. 8c) and successfully powered green LED bulbs in these states (Fig. 8d).

Oh and co-workers reported an intertwined nanosponge solid-state polymer electrolyte (INSPE) for FLIBs. The INSPE was conjugated with intertwined nanosponge (IN) of poly(vinylidene fluoride-*co*-hexafluoro-propylene) (PVDF-*co*-HFP) and ion-conducting polymer electrolyte (PE) containing poly(ethylene glycol)diacrylate (PEGDA), succinonitrile (SCN) plasticizer, and lithium bis(trifluoromethanesulfonyl)imide (LiTFSI). The fabrication process of INSPE was divided into two steps, as shown in Fig. 8e. First, the porous IN was prepared *via* phase separation, as acetone rapidly evaporates after bar-casting of the PVDF-*co*-HFP in water–acetone solution. Afterward, the PE solution was poured onto IN and solidified through the ultraviolet (UV)-polymerization of PEGDA and free-standing INSPE, which maintained the high mechanical strength of PVDF-*co*-HFP, and good ionic conductivity of PE was thereby obtained. The pore size and the component configuration of PE were further optimized. In addition, 40-INSPE 1 : 2 (synthesized from 40 mg mL^{-1} of PVDF-*co*-HFP solution and PE including PEGDA and SCN in a ratio of 1 : 2) with the highest ionic conductivity of 1.04 mS cm^{-1} at 27 °C, was selected. 40-INSPE 1 : 2 was evaluated in an LFP half-cell, which exhibited a discharge capacity of 144 mA h g^{-1}, high coulombic efficiency of 87.3% after 200 cycles, and good rate capability at several current density values. Further evaluation of 40-INSPE 1 : 2 under deformation (see Fig. 8f) revealed excellent ionic conductivity retention after increasing the bending angle to 85° or repeated bending, rolling, and folding cycles. A pouch cell with 40-INSPE 1 : 2 laminated between LFP and Li foil successfully lit up the LEDs under bending, rolling, and double folding, as shown in Fig. 8g.

As another approach, Zheng and co-workers demonstrated a Li-metal composite yarn (LMCY) as a flexible anode for wire-type FLIBs. The LMCY was fabricated *via* infusion of molten Li into a flexible and lithiophilic Cu–C yarn as shown in Fig. 8h.[111] The pristine carbon yarn was a twist of ~200 fibers, each with a diameter of 10 μm. The C yarn was already flexible and provided enough capillarity to liquids that wet its surface, but was lithiophobic as indicated by the large contact angle (120°) with the molten Li. To obtain a lithiophilic yarn, Cu (with a contact angle of 30°) was further coated *via* polymer-assisted metal deposition with a uniform thickness of 200 nm onto each carbon fiber. The LMCY exhibited much lower linear resistance (~1 ohm cm^{-1}) than the carbonaceous materials (*e.g.*, ~20 ohm cm^{-1} for the C yarn) and similar overpotentials even for different lengths of the yarn, due to the highly conductive Cu–C yarn. The LMCY also exhibited a stable overpotential of ~94 mV for more than 400 h, thereby outperforming the Li metal wire. Wire-type FLIBs were assembled with the LMCY as the anode and LFP or S yarn as the cathode (Fig. 8i). The cathode was fabricated by dripping the active material slurry onto the nickel-coated carbon yarn. The as-prepared electrodes were aligned in parallel, electrically isolated by a polypropylene separator, and encapsulated in a polyolefin tube, as shown in Fig. 8j. The battery delivered an initial capacity of 150 mA h g^{-1} and showed a high capacity retention of 76% after 400 cycles. In addition, the battery maintained its performance in the folded state and was able to power 36 LEDs even under knotted conditions (Fig. 8k). Wire-type materials could be directly woven with cotton yarns to create wearable power fabrics (see Fig. 8l). The battery textile, consisting of six LFP||LMCY fibers connected in parallel, delivered a capacity of 1 mA h cm^{-2} (Fig. 8m).

3.2 Supercapacitors

In general, supercapacitors (SCs) are divided into two types: pseudocapacitors and electrochemical double layer capacitors (EDLCs). Transition-metal oxides are one of the most promising candidates, for pseudocapacitors, because they provide high energy density through the redox reactions occurring within the bulk material.[19,112–119] Conductive polymers are also promising candidates.[120] However, for EDLCs, the electrical energy is stored by electrostatic accumulation on the interfacial electrolyte/electrode surface, mainly for carbon-based materials with a high specific surface area. Nowadays, supercapacitors have gained increasing attention in the field of wearable devices due to their electrochemical stability, long cycle life, exceptionally high charge–discharge speed, and safety. Electrodes, as one of the components of a supercapacitor (electrodes, separator, electrolyte, current collector, and packing shell), seem to have a considerable impact on the electrochemical performance of the capacitor. Thus, various electrode materials, including activated carbon,[121–124] CNTs,[117,125,126] CNFs,[127–130] graphene,[76,131–134] and MOFs,[135–138] have been developed.

Xu and co-workers reported that excellent mechanical properties were obtained for conductive metal–organic framework (c-MOF) nanolayers on cellulose nanofibers (CNFs), with hierarchical micro–mesoporosity, serving as electrodes in a foldable supercapacitor.[139] Fig. 9a shows a schematic of the synthesis process for the CNF@c-MOF hybrid nanofibers. First, the extracted CNFs from the green algae were subjected to TEMPO oxidation (TEMPO = 2,2,6,6-tetramethylpiperidin-1-yloxyl) aimed at developing carboxyl surfaces and achieving ion exchange with Ni^{2+} ions. Afterward, an aqueous solution containing an organic ligand (HTTP) was added for the construction of Ni-HTTP and a homogeneous suspension of CNF@c-MOF nanofibers was obtained. The electrochemical performance of the electrodes under mechanical deformation was evaluated by obtaining cyclic voltammetry (CV) curves under different folding angles (0°, 90°, 120°, and 180°). The results revealed (Fig. 9b) that folding the device had no influence on the CV curves within the potential windows (0–0.7 V) considered (scan rate: 100 mV s^{-1}). Fig. 9c shows a red LED that can be powered by bent or even folded devices.

As another method of fabricating foldable electrodes for supercapacitors, Zheng and co-workers fabricated new free-standing and foldable electrodes made of pure carbon and

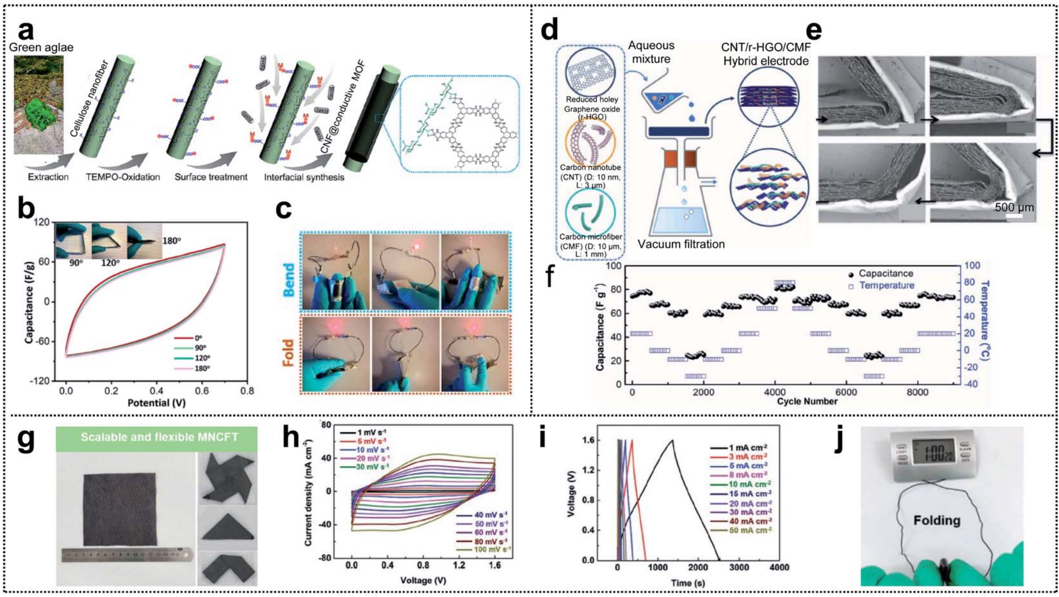

Fig. 9 Supercapacitor. (a) Schematic of the synthesis procedure of CNF@c-MOF hybrid nanofibers. (b) Cyclic voltammetry curves (scan rate: 100 mV s^{-1}) at different folding angles. (c) Photograph of a LED powered by the devices in series under different deformations. Reproduced from ref. 139. Copyright 2019, American Chemical Society. (d) Schematic illustration of the preparation of LPCSs. (e) A set of cross-sectional SEM images of a foldable film showing a recovery process. (f) Low-temperature foldability of SCs made with LPCSs. Reproduced from ref. 140. Copyright 2019, Wiley-VCH. (g) Optical images of large-scale MNCFTs and flexibility exhibition. (h) Cyclic voltammetry curves measured at different scan rates between 0 and 1.6 V. (i) Galvanostatic charge–discharge curves collected at different current densities between 0 and 1.6 V. (j) Images of textile-based electrochemical energy storage devices driving an electronic watch at the folding state. Reproduced from ref. 113. Copyright 2020, Wiley-VCH.

referred to as lamellar porous carbon stacks (LPCSs).[140] A uniform and free-standing LPCS (hybrid electrode) was obtained through vacuum filtration of an aqueous solution including HRGO nanosheets, CNTs, and CFs (Fig. 9d). The thickness of each layer and the space between the layers in the resulting multilayer lamellar structure were ~20 μm and 50 μm, respectively. To confirm foldability, they showed the structural change in the LPCS during a folding and unfolding cycle (see Fig. 9e). The lack of fractures or cracks (even at a small folding radius of <20 μm) may have resulted from the dissipation of inner compressive stress and outer tensile stress by the gaps between neighboring layers. Furthermore, based on the highly stable LPCS and the low-temperature-tolerant ionic liquid used as the electrolyte, they assessed the electrochemical performance of LPCS SCs over a wide range of temperatures (80 °C to −30 °C; see Fig. 9f). They performed 500 cycles at each temperature stage (capacitance values of 76.8, 67.4, 61.4, and 25.2 F g^{-1} obtained at 20 °C, 0 °C, −10 °C, and −30 °C, respectively). After the repeated temperature change, the specific capacitance of the LPSC SCs easily recovered its original value (73.6 F g^{-1}), indicating excellent structural integrity and good stability of the SCs at various temperatures.

Owing to their high conductivity, good flexibility, and good mechanical properties, carbon fiber textiles (CFTs) are a promising candidate for substrates used in the loading of active materials. Yuan and co-workers fabricated tailorable, wearable, and foldable solid-state asymmetric supercapacitors (ASCs) based on CFTs.[113] The suggested positive and negative electrodes of the ASCs were O/N-functionalized CFTs (ONCFTs) and N-doped CFTs with MXene ink (MNCFTs), respectively, and polyvinyl alcohol (PVA)/H_2SO_4 gel electrolytes were inserted between the electrodes. Fig. 9g shows a 10 × 10 cm^2 region of the MNCFT electrodes with different folded shapes. The lack of fractures demonstrates the excellent flexibility and mechanical stability of these electrodes. Furthermore, they compared the operating potential windows of the MNCFT (−0.6 to 0.3 V) and ONCFT electrodes (0 to 1 V) with that of the assembled ASC, which is capable of extending the voltage window to 1.6 V. Based on the extended voltage window, ASCs exhibited undistorted CV shapes even at a high scan rate of 100 mV s^{-1}, indicating high rate capability (Fig. 9h). Additionally, the galvanostatic charge–discharge profiles were only slightly distorted compared with the ideal symmetric triangular shape (current density: 1–50 mA cm^{-2}) suggesting good reversibility and pseudocapacitive properties (Fig. 9i). The excellent rate capability resulted in 60% capacitance retention (548 and 330 mF cm^{-2}) even when the scan rate was increased from 10 to 100 mV s^{-1}. For practical applications, the textile-based electrochemical energy-storage-devices were able to power an electronic watch under repeated folding conditions, thereby demonstrating good flexibility and excellent integrity (Fig. 9j).

3.3 Air batteries

Metal–air batteries are potential candidates for foldable batteries with high energy density.[141,142] For example, Li–air and Zn–air batteries are promising for next-generation energy-storage-devices (such as electric vehicle batteries) due to their excellent power storage capacity, safety, low cost, and abundant materials.[143,144] Li–air batteries have a high theoretical energy density (3500 W h kg^{-1}).[145] However, these batteries are plagued by problems such as low charge/discharge efficiency, unstable electrolyte of partial discharge products, and dendrite formation of unstable anodes.[146,147] Many studies have focused on overcoming these issues. For example, Feng and co-workers developed a foldable Li–air battery (LAB) using two approach strategies (Fig. 10a),[148] namely the design of a stable anode and the utilization of gel-polymer electrolyte (GPE). For a stable anode, reduced graphene oxide (rGO) played a critical role in alleviating the Li dendrite formation and increasing the

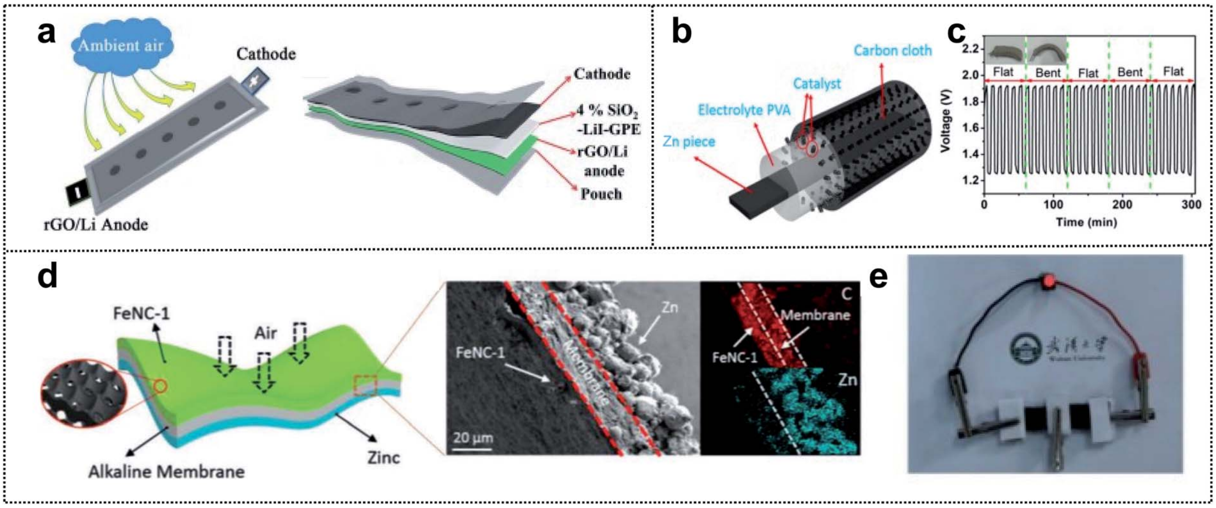

Fig. 10 Foldable air batteries. (a) Schematic illustration of the flexible belt-shaped Li–air battery structure. Reproduced from ref. 148. Copyright 2018, Royal Society of Chemistry. (b) Schematic illustration of a solid-state Zn–air battery. (c) Stability of the solid-state rechargeable Zn–air batteries under flat and folded states. Reproduced from ref. 148. Copyright 2018, Elsevier. (d) Schematic illustration of a substrate-free flexible ZAB. (e) Digital image of the red-light LED powered by two tandem devices. Reproduced from ref. 153. Copyright 2019, Wiley-VCH.

flexibility and mechanical strength. A GPE with 4 wt% SiO_2 and LiI imparted a high ionic conductivity (1.01 mS cm^{-1}) and reduced the air-attacking-induced Li passivation. Moreover, LiI and SiO_2 assisted in the prevention of discharge products and improved the flame resistance. For a fixed capacity of 500 mA h g^{-1}, the SiO_2–LiI–GPE-based LAB exhibited a lower voltage than the SiO_2–GPE-based LAB (100 cycles *vs.* 59 cycles for a discharge terminal voltage >2.0 V). This result indicated that LiI additives in the GPE could improve the reversibility of LABs. In addition, the SiO_2–GPE-based flexible belt-shaped LAB exhibited a long cycle life of 100 cycles with a small voltage gap of ~1.45 V and powered a red LED under twisting to 90° or 360°.

Similar to LABs, rechargeable Zn–air batteries have a high theoretical energy density (1086 W h kg^{-1}).[149] However, some catalysts with platinum (Pt) or iridium (Ir) in the air cathode are expensive, rare, and have low electrochemical stability in Zn–air batteries.[150,151] The relatively low kinetics of the oxygen reduction reaction (ORR) and oxygen evolution reaction (OER) at the cathode can be overcome by developing electrochemical catalysts that will yield high-performance foldable Zn–air batteries.[152] In order to enhance the catalytic effect for the ORR and OER in these batteries, Cao and co-workers designed a solid-state Zn–air battery using single-atom cobalt electrocatalysts for high performance.[153] They utilized Zn, CC, and PVA as the anode, current collector, and PE to prevent leakage of liquid devices for foldable batteries (Fig. 10b). In addition, the single-atom Co–N–C composite (CoN_4/NG) was used as a high-performance electrocatalyst with a low overpotential (0.74 V, E_{ORR}–E_{OER}). The ORR onset potential of CoN_4/NG (0.98 V) was considerably higher than that of Co-NPs/NG (0.92 V). The assembled foldable Zn–air battery was characterized by excellent discharging and charging properties (730 *vs.* 711 mA h g^{-1} for commercial Pt/C) with a high power density, energy density (671 W h kg^{-1}), and long stability (6 h in flat and folded states) (Fig. 10c). Chen and co-workers reported an alkaline polymer membrane-based foldable Zn–air battery.[154] In this work, two strategies (self-standing active layer and gel-electrolyte coated separators) were employed through an ink-casting/hot-pressing approach for obtaining a high-performance flexible battery (Fig. 10d). An interconnected Fe/N-doped 3D carbon-based electrocatalyst was used as an ultrathin cathode material without the backing gas-diffusion layer for outstanding catalytic properties. Moreover, a three-in-one design with Zn powder, an alkaline polymer membrane, and electrocatalysts achieved a large ion exchange capacity (1 mmol g^{-1}), high ionic conductivity (>0.1 S cm^{-1}), chemical stability, and outstanding mechanical properties for flexible electrodes. Consequently, the all-solid-state foldable Zn–air battery exhibited excellent flexibility and exceptional battery performance (power density of 250 mW cm^{-3} and a high capacity of 150.4 mA h cm^{-3} at a fast-discharging rate of 8.3 mA cm^{-3}) (Fig. 10e). Therefore, the specific design of highly active electrocatalysts and a flexible polymer-based membrane, as well as the appropriate combination of current collectors and packing agents, can yield high-performance foldable air batteries.

3.4 Multi-valent batteries

Multi-valent batteries such as Zn or Al-ion batteries have attracted great interest due to low-cost, high-power density, and high capacity.[155,156] Compared with Li- and Na-ion batteries, multi-valent batteries can have double or triple capacities for the same number of ions because the number of ions that react at the electrodes decreases within the electrolyte when we substitute M^+ with M^{n+} (n = 2 and 3) charge carriers.[157] In addition, multi-valent metals such as Zn, Ca, Mg or Al are abundant in nature.[158] This means that multi-valent batteries

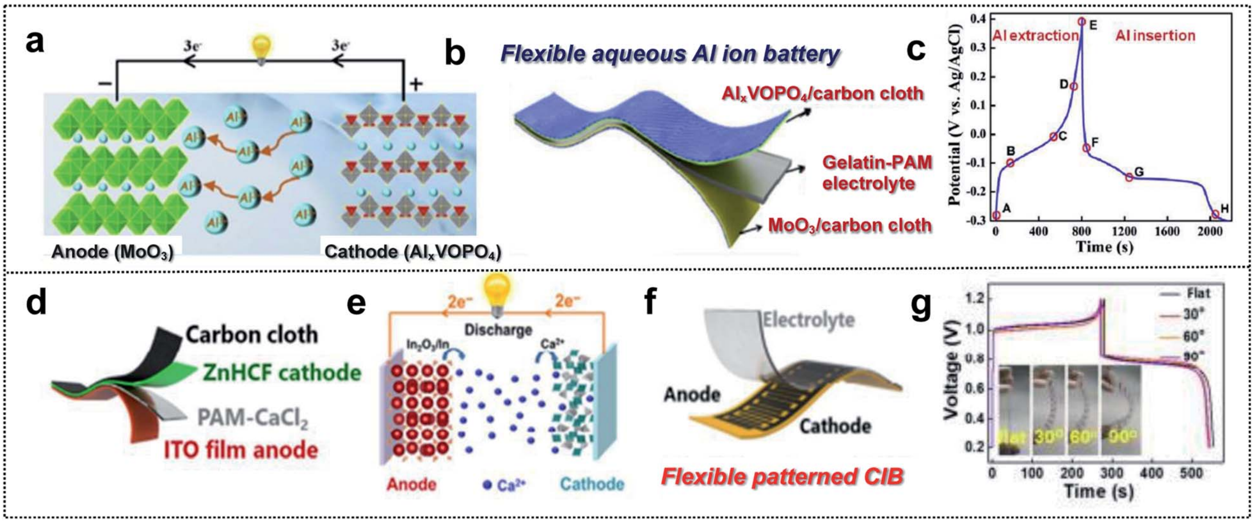

Fig. 11 Foldable multi-valent batteries. (a) Schematic illustration of the working principle of aqueous AIBs based on the intercalation electrode. (b) Schematic illustration of a flexible aqueous AIB. (c) Charge/discharge curves of $VOPO_4$ at a current density of 1 A g^{-1}. Reproduced from ref. 163. Copyright 2020, Elsevier. (d) Schematic illustration of a flexible aqueous CIB, (e) working principle schematic of aqueous CIB, (f) schematic illustration of a flexible patterned CIB and (g) GCD curve of a flexible CIB at different bending angles. Reproduced from ref. 167. Copyright 2021, Springer Nature.

can serve as next-generation wearable and foldable energy-storage-devices that overcome issues regarding the battery cost, energy density, power density, and resources.[159–161] Despite these advantages, Al ion batteries (AIBs) suffer from the kinetics limitation of Al^{3+}, which is associated with slow ion insertion and extraction.[162] The selection of electrode materials is therefore very crucial. Huang and co-workers obtained a safe flexible aqueous AIB for wearable electronic devices with long cycling stability, high capacity, and good rate capability using an Al_x-$VOPO_4$ cathode, a MoO_3 anode, and a gelatin–polyacrylamide hydrogel electrolyte (Fig. 11a and b).[163] $VOPO_4$ enabled fast cation intercalation, owing to the coordination of the V atom (Fig. 11c). Furthermore, MoO_3 is a 2D layered structure with good electrochemical intercalation and easy coupling of multivalent-state Mo atoms. Grafted polymer electrolytes with gelatin and polyacrylamide (PAM) provided flexibility and a high ionic conductivity (20.83 *vs.* 0.65 mS cm^{-1} for PVA–H_3PO_4 gel electrolyte). Consequently, this foldable AIB exhibited good durability (86.2% after 2800 cycles), a high specific capacity (88 mA h g^{-1}), and a high rate capability (6 A g^{-1}). This indicates that flexible AIBs capable of overcoming low kinetics possess considerable potential for wearable devices used as foldable batteries.

Due to a moderate charge density and polarization strength, Ca-ion batteries (CIBs) are characterized by better kinetics than that of the batteries based on other multi-valent ions.[164,165] However, the number of electrode materials capable of hosting Ca^{2+} cations is limited. For example, layered potassium birnessite ($K_{0.31}MnO_2\cdot 0.25H_2$), a well-established host material, exhibits low rate capability and fast capacity drops (51%) for the initial 20 cycles, owing to poor kinetics and instability.[166] Huang and co-workers used the Sn-doped In_2O_3 (ITO) film as the aqueous CIB anode with a zinc hexacyanoferrate (ZnHCF) cathode (Fig. 11d).[167] In this system, an ITO electrode assisted the insertion/extraction reaction of Ca cations in the reduction of In^{3+} for charge balance. Ca^{2+} intercalation/deintercalation occurred during the partial reduction of Fe^{3+} to Fe^{2+} in the ZnHCF cathode and the conversion reaction at the ITO anode (Fig. 11e). For the foldable CIB, they utilized PAM/$CaCl_2$ as the GPE and ZnHCF/CC as flexible electrodes (Fig. 11d). This well-designed flexible CIB exhibited a high specific capacity of 75.3 mA h g^{-1} at 0.4 A g^{-1} and high coulombic efficiency of 97.5%. In addition, excellent foldable properties for powering an electronic watch in a flat or bending state were realized (Fig. 11f and g). Regarding multi-valent batteries, optimized electrode materials should be considered. Moreover, the cell configuration of GPE, flexible substrates, and mechanically stable electrode materials is significant for foldable batteries.

4. Analysis

4.1 Electrochemical characterization

Electrochemical characterization of foldable batteries is the same as that of conventional batteries, except for an additional analysis confirming that the system performance is maintained even in the folded state. Previous studies have already performed the aforementioned analysis process implicitly, but the basic guideline is still necessary for researchers who will start investigations of foldable battery systems. Two examples are introduced in this section as a means of proving a common guideline for evaluating foldable electrodes or separators.

Foldable electrodes usually have non-conventional electrode structures because rigid metal current collectors are unsuitable for use under deformation conditions. Therefore, the electrical conductivity of these electrodes should be comparable to that of metal current collectors in both the unfolded and folded states. Song and co-workers reported similar findings for active material loaded silver-nanowire-wound microfiber (AgNW$MF) or carbon-nanotube-webbed microfiber (CNT#MF) electrodes for FLIBs.[55] The electrical conductivity of the as-fabricated electrodes was measured in the unfolded state and also tracked as a form of resistance change during repeated folding cycles, as shown in Fig. 12a. The conductivity of LTO-loaded AgNW$MF was four orders of magnitude higher than that of a practical LTO-slurry coated aluminum electrode and the resistance was consistent for 1000 folding cycles. The lithiation/delithiation electrochemistry and rate capability of the electrodes were further analyzed in a half-cell including lithium metal used for panels (Fig. 12b). Compared with LTO-loaded AgNW$MF, the foldable electrode exhibited a similar capacity retention but with a higher gravimetric capacity and good rate capability due to the low weight of the electrode and excellent electrical conductivity, respectively. The same analysis was performed for two- and four-time folded electrodes that were assembled into pouch-type half-cells, as shown in Fig. 12c. LFP-loaded CNT#MF and LTO-loaded AgNW$MF were assembled into pouch-type full cells and tested after confirming the electrochemical performance of the electrodes in the unfolded and folded states (Fig. 12d). To confirm that the electrochemical performance was maintained under deformation conditions (see Fig. 12e), the relative capacity was measured during charge/discharge cycles with intermittent 20 folding and unfolding events every 20 cycles. The cell exhibited excellent capacity retention even when four-time folded electrodes were used. Moreover, LED bulb show-up was demonstrated after folding, crumpling, and hammering (Fig. 12f).

GPEs and solid-state electrolytes (SPEs) are widely used as both electrolytes and separators for foldable batteries due to their high mechanical durability and non-susceptibility to electrolyte leakage.[168–171] The ionic conductivity of GPEs and SPEs directly affects the whole cell performance (the operating voltage, lifespan, and power output) and must therefore be sufficiently high.[172] Hu and co-workers demonstrated porous PVA-based GPEs for foldable zinc air batteries (FZABs) and showed a detailed electrochemical analysis process from the GPE step to a full cell test.[173] The GPEs were fabricated through a simple phase-inversion method and then sandwiched between zinc foil and a catalyst-loaded air electrode for FZAB assembly, as shown in Fig. 12g. The GPEs consisted of a PVA matrix immersed in a 6 M KOH solution and SiO_2 was introduced on the surface for increased water retention. Initial impedance spectra were measured for GPEs with different contents of the SiO_2 filler. Subsequently, the ionic conductivity was monitored over time to identify the optimum conditions

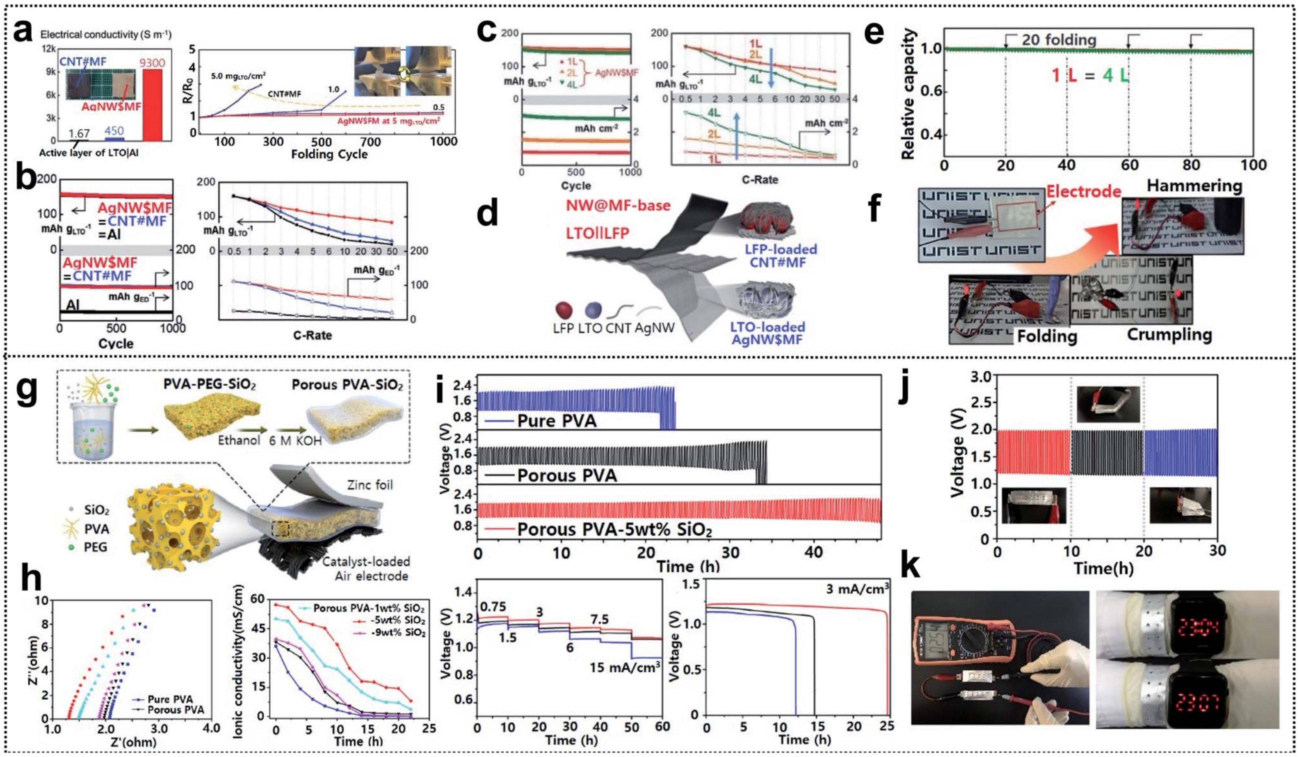

Fig. 12 Electrochemical characterization. (a) Initial electrical conductivities of LTO containing electrodes and resistance change along with repeated folding cycles, (b) lithiation electrochemistry of LTO loaded on AgNW$MF, CNT#MF, and aluminum foil, (c) capacity retention and rate capabilities of folded AgNW$MFs (2 L and 4 L) *versus* the unfolded one, (d) schematic image of a flexible LTO||LFP battery, (e) capacity retention of unfolded and folded batteries and (f) optical images of LEDs powered by a battery under folding, crumpling and hammering. Reproduced from ref. 55. Copyright 2017, Wiley VCH. (g) Schematic diagram of a foldable zinc–air battery (FZAB) and the preparation process, (h) impedance spectra and ionic conductivity of PVA-based GPEs, (i) several electrochemical characterization studies of FZABs based on various PVA-based GPEs, (j) cycle performance under different bending conditions and (k) open-circuit voltage demonstration with two FZABs in series and demonstration of a LED watch powered by bracelet-type FZABs. Reproduced from ref. 173. Copyright 2018, Elsevier.

that yield the highest ionic conductivity and electrolyte absorption capacity of GPEs (Fig. 12h). The resistance decreased with increasing SiO_2 filler content. However, over a certain point (9 wt%), excessive SiO_2 could lead to aggregation and disruption of the ion transport, thereby affecting the overall performance, as indicated by the high resistance and poor water retention properties. FZABs were assembled using optimized porous PVA-5 wt% SiO_2 GPEs and were then subjected to several galvanostatic charge/discharge measurements, as shown in Fig. 12i. The electrochemical performance (lifespan, rate capability, and specific capacity (maximum value: 68.0 mA h cm^{-3})) of the GPEs was superior to that of pure PVA or porous PVA. The cycle performance of FZABs with the GPEs was measured at bending angles of 0°, 60°, and 180° (Fig. 12j). The FZABs exhibited excellent stability, *i.e.*, the potential changed only modestly with the bending angle. Furthermore, two FZABs were connected in series in order to realize a high open-circuit voltage of 2.54 V, which was enough to power an LED watch even in the form of a bracelet, as shown in Fig. 12k.

4.2 Mechanical characterization

Several review papers reported significant progress in the field of foldable LIBs and supercapacitors (SCs) exhibiting high electrochemical performance and flexibility.[174–176] However, compared with the evaluation of electrochemical performance, diverse methods and parameters are employed for evaluation of the flexibility, and unified assessment criteria are lacking. Recently, various efforts have focused on precise and proper mechanical characterization of foldable energy-storage-devices (ESDs).[109,177–183] In this section, we discuss various measurement methods and their effectiveness in determining the mechanical properties of deformable ESDs.

Zhi and co-workers investigated the validity of the widely used parameters for bending durability and assessed the softness of flexible ESDs.[184] They proposed three parameters, θ (the bending angle), R (the bending radius of curvature), and L (the length of the device), for precise evaluation of the durability (see Fig. 13a). The figure shows that lowering the bending angle or bending radius increases the area of stress regions and the degree of the tensile/compressive strain on the outer/inner surface. Similarly, for a given bending angle and bending radius, they suggested that (compared with a shorter device) a longer device may be less affected by bending as the stressed region is localized. To demonstrate the effects of the parameters, they compared the dependence of capacity retention during cycling on different bending parameters (θ, R, and L).

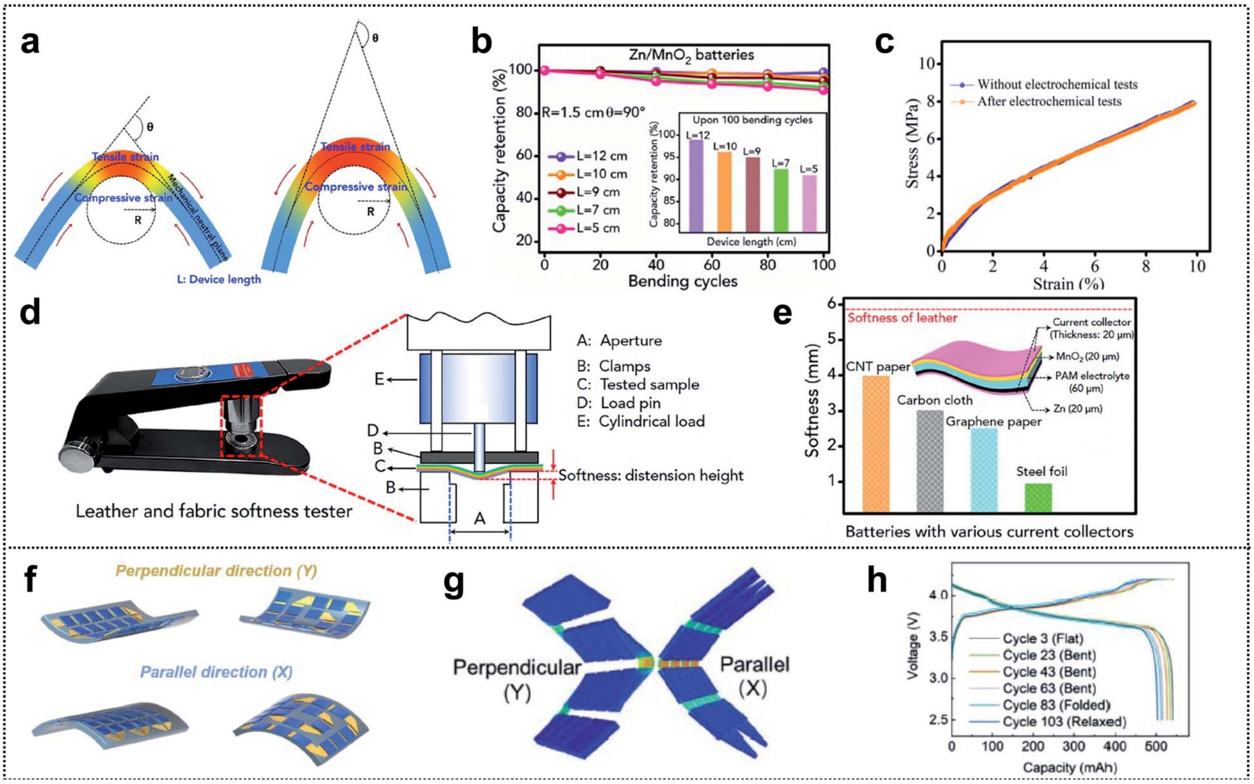

Fig. 13 Mechanical characterization. (a) Schematics of structures and the three key parameters (L, θ, and R) that are commonly used to demonstrate the bending state of flexible and wearable energy storage devices (ESDs). (b) Zn–MnO$_2$ batteries with different lengths at a certain bending angle (90°) and bending radius (1.5 cm). (c) Stress–strain curve of flexible Zn/MnO$_2$ batteries before and after electrochemical tests (100 charge/discharge cycles). (d) Photograph of the softness tester and schematic illustration for measuring softness. (e) Softness of flexible Zn–MnO$_2$ batteries constructed with different flexible current collectors (the inset shows the schematic illustration of the structure of flexible Zn–MnO$_2$ batteries and the thickness of different components). Reproduced from ref. 184. Copyright 2019, Elsevier. (f) Schematic illustration of the different types of snake-origami batteries with bidirectional deformation. (g) Finite element calculations of snake-origami batteries in the bending state with bidirectional deformation: parallel (X) and perpendicular (Y) directions. (h) The cycle performance of snake-origami batteries in different states: flat, bent, fold, and relaxed state under a constant current density of 0.5C. Reproduced from ref. 188. Copyright 2021, Wiley-VCH.

Fig. 13b shows the cycle retention of Zn/MnO$_2$ batteries for a fixed bending radius and bending angle (1.5 cm and 90°, respectively) and different lengths. When the length of the device decreased from 12 cm to 5 cm, the capacity retention for 100 cycles decreased from ∼99% to ∼91%. This capacity decay of the cell was attributed to cracks in the electrodes and interfacial contact deterioration induced by the repeated mechanical deformation, *i.e.*, mechanical tests affect the electrochemical performance. However, they confirmed the mechanical properties after the electrochemical tests and the stress–strain curve revealed a negligible effect on the mechanical properties of ESDs (Fig. 13c). In addition, they discussed the wearability and comfort assessment of a flexible ESD in terms of softness. They proposed softness as a parameter for evaluating the softness of such ESDs, which can be evaluated using a commercially available leather and fabric softness tester, as shown in Fig. 13d. During the evaluation, a cylindrical load of defined mass was lowered at a specified rate onto a securely clamped area of the ESD and the distension from the ESD was recorded as the softness (unit: mm). Foldable current collectors are an inevitable component of foldable ESDs with high softness. Thus, they measured the softness of flexible batteries using different current collectors such as CNT paper, CC, graphene paper, and steel foil (Fig. 13e). The highest value of softness (4.06 mm) was obtained for batteries with CNT paper (current collectors in descending order of softness: CNT paper, CC, graphene paper, and steel foil).

In addition to mechanical characterization through the actual deformation of a foldable ESD, mathematical analysis (computational tools) of the detailed deformation has rapidly been developed with significant evolution of computer technology. Finite element analysis (FEA), a numerical method, provides the stress distribution of a foldable ESD by formulating and combining the algebraic equations of sub-units. In FEA simulation, a continuous complex structure is discretized into finite elements and a fine element mesh is generated by connecting the fine elements involving material and structural properties. Based on the density of the mesh, the strain distribution between the different deformation states and different structures can be measured.[111,185–187]

Song and co-workers reported a novel bidirectional snake-origami battery with a scalable planar structure, which was

Table 1 Summary of features of foldable energy storage systems, such as system, active materials, electrolytes, capacity, active material mass loading, cycle stability, and energy density

System$^{\text{ref.}}$	Active materials (cathode/anode)	Electrolyte	Capacity	Mass loading (mg cm^{-2})	Cycle stability	Energy density
Lithium ion-battery[43]	LCO@CNT//GeO$_x$/ZnO/C	1 M LiPF$_6$ in EC/DMC/DEC (1 : 1 : 1, v/v/v)	890 mA h g^{-1}	1.2	464 mA h g^{-1} over 500 cycles at 1 A g^{-1}	—
Potassium-ion battery[44]	(KFe^{II}[(Fe^{III}(CN)$_6$)])//SnS$_2$@C	0.8 M KPF$_6$ in EC/DEC (1 : 1, v/v)	457.4 mA h g^{-1}	1.2	183.1 mA h g^{-1} after 1000 cycles at 2 A g^{-1}	—
Aluminum-ion battery[45]	Co$_9$S$_8$@CNT–CNF//-	AlCl$_3$ and [EMIm]Cl	315 mA h g^{-1}	1.5	87 mA h g^{-1} after 6000 cycles at 1 A g^{-1}	300 W h kg^{-1}
Lithium ion-battery[55]	CNT#MF@LFP//AgNW$MF@LTO	1 M LiPF$_6$ in EC/DEC (3/7, w/w)	150 mA h g^{-1}	5.0	150 mA h g^{-1} after 1000 cycles at 1C	—
Lithium ion-battery[74]	LMO//titania/rGO	1 M LiPF$_6$ in EC/DEC (1 : 1, v/v)	168 mA h g^{-1}		100 mA h g^{-1} after 100 cycles at 0.017 mA	—
Lithium–sulfur battery[75]	GO@sulfur@PEDOT:PSS//Li foil	1 M Li$_2$S$_6$ in DOL/DME (1 : 1, v/v)	1584 mA h g^{-1}	2.0	(80%) 806 mA h g^{-1} after 500 cycles at 1C	—
Lithium–sulfur battery[82]	MF@Ti$_3$C$_2$T$_x$/S//Li foil	0.1 M Li$_2$S$_6$ and 1 M LiTFSI in DOL/DME (1 : 1, v/v)	916 mA h g^{-1}	1.5	674 mA h g^{-1} after 1000 cycles at 1C	—
Zinc-ion battery[83]	LMO//MXene/graphene@Zn	PVA@MXene	126 mA h g^{-1}	25	90.3% capacity retention for 60 cycles at 2C	—
Zinc-ion battery[91]	NVO//AgNPs@CC/Zn	1 M Zn(CF$_3$SO$_3$)$_2$ aqueous solution	321 mA h g^{-1}	4	184 mA h g^{-1} after 1200 cycles at 5 A g^{-1}	—
Lithium-ion battery[101]	LCO//graphite	1 M LiPF$_6$ in EC/DEC (1 : 1, v/v)	151.4 mA h g^{-1}	12.29	145.7 mA h g^{-1} after 20 cycles at 0.2C (flexed state)	242 W h L^{-1}
Lithium-ion battery[102]	LCO//graphite	1 M LiPF$_6$ in EC/DEC (1 : 1, v/v)	132.9 mA h g^{-1}	—	131.5 mA h g^{-1} after 50 cycles at 1C (dynamic bending and twisting)	371.9 W h L^{-1}
Lithium-ion battery[103]	LCO//graphite	1 M LiPF$_6$ in EC/DEC (1 : 1, v/v)	148.6 mA h g^{-1}	12.8	124.2 mA h g^{-1} after 15 cycles at 1C (dynamic folding)	245 W h L^{-1}
Lithium-ion battery[109]	LFP//lithium metal	Intertwined nanosponge solid-state polymer electrolyte	144 mA h g^{-1}	6.0	87.3% capacity retention after 200 cycles at 0.2C	—
Lithium–metal battery[111]	Yarn-like LFP//Li–metal composite yarn	1 M LiTFSI in DOL/DME (1 : 1, v/v) + 2 wt% LiNO$_3$	150 mA h g^{-1}	1.2	88% capacity retention after 170 cycles	292.4 W h L^{-1}
Supercapacitor[113]	MNCFT//ONCFT	PVA/H$_2$SO$_4$ gel electrolyte	148 F g^{-1}	3	90% capacitance retention after 30 000 cycles at 50 mA cm^{-2}	277.3 μW h cm^{-2}
Supercapacitor[139]	CNF@c-MOF//CNF@c-MOF	PVA/KCl gel electrolyte	75 F g^{-1}	0.7	90% capacitance retention after 10 000 cycles at 1 A g^{-1}	—
Supercapacitor[140]	LPCS (lamellar porous carbon stack)//LPCS	BMIMBF$_4$ electrolyte	65 F g^{-1}	20.2	95% capacity retention after 10 000 cycles at −30 °C	2.1 mW h cm^{-2}
Lithium–air battery[148]	Air//rGO/Li	4% SiO$_2$–LiI–GPE	500 mA h g^{-1}	1.0	Average voltage gap of 1.45 V during 100 cycles	—
Zinc–air battery[153]	Air//CoN$_4$/NG/Zn	6 M KOH and 0.2 M ZnO	730 mA h g^{-1}		100 hours	671 W h kg^{-1}
Aluminum-ion battery[161]	VOPO$_4$//MoO$_3$	Gelatin–polyacrylamide hydrogel electrolyte	73 mA h g^{-1}	1.5	86.2% capacity retention after 2800 cycles at 1 A g^{-1}	—
Calcium-ion battery[165]	ZnHCF//Sn-doped ITO	Polyacrylamide hydrogel electrolyte	71.2 mA h g^{-1}	0.8	75.3 mA h g^{-1} at 0.4 A g^{-1}	—

obtained by separating the energy-storage and mechanical deformation segments (Fig. 13f).[188] FEA of the deformation at soft connecting segments was used to elucidate the mechanical durability of the batteries. Fig. 13g shows that the batteries with 4 × 4 arrays were bent along two directions and the stress was concentrated only on the soft segments, rather than on the energy-storage segments. Moreover, *via* simulations, they determined the effectiveness of the battery flexibility and the relationship between the energy density and the minimum bending radius as a function of the dimensionless gap width. Based on the mechanical characterization, they evaluated the performance of the batteries in various mechanical deformation states including flat, bent, folded, and relaxed. The voltage profiles of each cycle (see Fig. 13h) revealed negligible capacity degradation (0.066% for each cycle) or overpotential, indicating the excellent flexibility of the snake-origami batteries.

5. Outlook and perspective

In this review, we briefly cover state-of-the-art and some pioneering studies on the foldable ESDs reported so far. This review highlights the morphologies of materials (1D, 2D, 3D, and structural design) for foldable electrodes and discusses the foldable ESDs (Li-ion batteries, supercapacitors, air batteries, and multi-valent batteries). Furthermore, beyond foldability, this review discusses the evaluation methods (electrochemical and mechanical analysis) for these devices. The features of various strategies for different foldable ESDs based on the system, active materials, electrolytes, capacity, active material mass loading, cycle stability, and energy density are summarized in Table 1. Although considerable progress has already been accomplished in this area, challenges (including low energy density, high cost, poor productivity, packaging materials, and safety issues) are encountered in the practical application and commercialization of these devices. Thus, in this chapter, we discuss the challenges and perspectives for the future improvement of foldable ESDs.

Firstly, the energy density ($\mathrm{W\ h\ L^{-1}}$ or $\mathrm{W\ h\ g^{-1}}$) is closely related to the lifetime and portability of electronic devices and is hence the most important factor for evaluating the performance of energy devices. This is especially crucial for wearable devices (such as smart watches, smart lenses, and electronic patches) where a long lifespan associated with their operating hours and portability is required. In this context, the working voltage, capacity, weight, and volume should be carefully considered in order to achieve a high energy density. Foldable energy devices, unlike conventional ESDs, need electrochemically inactive components, which provide foldability to the whole device. Unfortunately, these components usually lower the energy density of the devices and can even lead to deterioration of the electrochemical performance. Thus, the electrode of foldable ESDs should be composed of all-electrochemically active materials. The weight fractions of the electrolyte, separator, and packaging materials in these devices will probably be reduced in order to obtain a high energy density. In addition, a high mass loading of active materials is needed for realizing a high energy density and can be simply achieved by increasing the film thickness. The drawbacks resulting from thick electrodes (including low foldability and inefficient ion diffusion) can be overcome by a well-engineered porous structure containing moderate space for the mechanical strain and the electrolyte near the active materials.[75,189–193]

Secondly, the high cost of the materials and poor productivity of foldable ESDs should also be considered. Substrates for foldable electrodes such as graphene, CC, and CNT paper have good electrical conductivity and mechanical properties but their high cost, compared with that of the conventional substrates (*e.g.*, copper and aluminum foil), impede the commercialization of foldable ESDs. Additionally, the large-scale production of foldable electrodes and their substrates is quite challenging, although laboratory-scale production for assembling various prototypes of foldable ESDs is quite straightforward. The current large-scale coating or deposition technologies (*e.g.*, roll-to-roll coating) were developed for rigid substrates and not adapted to foldable substrates for loading active materials.

Thirdly, packaging materials of foldable ESDs are frequently neglected. Metal cases are required to prevent the air and moisture penetration in battery packaging. For example, during the washing of wearable electronics, water and laundry detergents, which can cause severe damage to the batteries, may penetrate the batteries as existing packaging materials and technologies are ineffective in protecting the batteries. Moreover, although the foldability of electrodes, separators, and current collectors is assured, the packaging must also provide the same level of foldability to maintain the battery system under severe deformation. The modification of packaging materials with the aim of preserving the integrity of foldable ESDs under various deformations should therefore be seriously considered as a means of releasing the strain in metal layers.

Lastly, the electrochemical performance and durability of foldable ESDs under extreme conditions should be investigated for practical applications. The previously reported studies have focused only on the performance of foldable ESDs in ambient environments. The performances under harsh conditions, such as extremely high humidity, underwater environments, high pressure, and high/low temperatures, are rarely reported.[94,194–196] Moreover, under various harsh conditions, inevitable issues (including leakage, flammability, and volatility) associated with organic-based liquid electrolytes and related to the safety of devices are encountered. Non-flammable aqueous electrolytes are good candidates for overcoming these issues. However, the low operating voltage resulting from the irreversible decomposition (oxygen evolution reaction and hydrogen evolution reaction) of aqueous electrolytes hinders realization of high energy density foldable systems.[83,197,198] Replacing conventional flammable liquid electrolytes with solid-state electrolytes can provide improved safety and integrity but challenges such as low ionic conductivity and side reactions between the electrode/electrolyte interfaces are encountered.[20,109,112,153,199]

In summary, although numerous efforts have been made to develop foldable ESDs for commercialization, many hurdles still remain to hamper the further approaches near to commercialization. Low energy density, high cost with poor productivity, ignorance of packaging materials, and insufficient evaluation conditions are included as main issues for significant improvements in this field. Among them, critical challenges in terms of durability and performance of foldable batteries are low energy density and insufficient evaluation conditions. To handle the former challenge, one possible key can be to reduce the fraction of inactive components for decreasing the weight/volume of the cells and the other key can be to use high-capacity active materials such as alloy-type (*e.g.*, silicon, germanium, and tin) lithium metal anodes, and sulfur cathodes for increasing the energy. Also, constructing parameters and criteria for the extreme conditions (*e.g.*, humidity, low/high temperature, and external shock) should be considered for determining precise durability, performance, and safety under the certain conditions. It is believed that the cost/productivity and packaging material issues can be resolved by fabricating appropriate flexible current collectors and flexible packaging materials with the combined efforts in materials science and electrochemistry.

Conflicts of interest

There are no conflicts to declare.

Acknowledgements

This work was supported by the National Research Foundation of Korea (NRF) grant funded by Ministry of Education (2019R1I1A1A01050857 and NRF-2021M3H4A1A02099354).

References

1 J. A. Rogers, Z. Bao, K. Baldwin, A. Dodabalapur, B. Crone, V. R. Raju, V. Kuck, H. Katz, K. Amundson, J. Ewing and P. Drzaic, *Proc. Natl. Acad. Sci. U. S. A.*, 2001, **98**, 4835–4840.

2 I. You, B. Kim, J. Park, K. Koh, S. Shin, S. Jung and U. Jeong, *Adv. Mater.*, 2016, **28**, 6359–6364.

3 W. J. Song, S. Yoo, G. Song, S. Lee, M. Kong, J. Rim, U. Jeong and S. Park, *Batteries Supercaps*, 2019, **2**, 181–199.

4 W. J. Song, S. Lee, G. Song, H. B. Son, D. Y. Han, I. Jeong, Y. Bang and S. Park, *Energy Storage Mater.*, 2020, **30**, 260–286.

5 S. I. Park, D. S. Brenner, G. Shin, C. D. Morgan, B. A. Copits, H. U. Chung, M. Y. Pullen, K. N. Noh, S. Davidson, S. J. Oh, J. Yoon, K. I. Jang, V. K. Samineni, M. Norman, J. G. Grajales-Reyes, S. K. Vogt, S. S. Sundaram, K. M. Wilson, J. S. Ha, R. Xu, T. Pan, T. I. Kim, Y. Huang, M. C. Montana, J. P. Golden, M. R. Bruchas, R. W. t. Gereau and J. A. Rogers, *Nat. Biotechnol.*, 2015, **33**, 1280–1286.

6 D. G. Mackanic, T. H. Chang, Z. Huang, Y. Cui and Z. Bao, *Chem. Soc. Rev.*, 2020, **49**, 4466–4495.

7 G. M. Zhou, F. Li and H. M. Cheng, *Energy Environ. Sci.*, 2014, **7**, 1307–1338.

8 T. Li, Z. G. Suo, S. P. Lacour and S. Wagner, *J. Mater. Res.*, 2005, **20**, 3274–3277.

9 S. Wagner, S. P. Lacour, J. Jones, P. H. I. Hsu, J. C. Sturm, T. Li and Z. G. Suo, *Phys. E*, 2004, **25**, 326–334.

10 Z. Song, T. Ma, R. Tang, Q. Cheng, X. Wang, D. Krishnaraju, R. Panat, C. K. Chan, H. Yu and H. Jiang, *Nat. Commun.*, 2014, **5**, 3140.

11 Z. Song, X. Wang, C. Lv, Y. An, M. Liang, T. Ma, D. He, Y. J. Zheng, S. Q. Huang, H. Yu and H. Jiang, *Sci. Rep.*, 2015, **5**, 10988.

12 K. K. Fu, J. Cheng, T. Li and L. B. Hu, *ACS Energy Lett.*, 2016, **1**, 1065–1079.

13 Z. H. Fang, J. Wang, H. C. Wu, Q. Q. Li, S. S. Fan and J. P. Wang, *J. Power Sources*, 2020, **454**, 227932.

14 A. Sumboja, J. Liu, W. G. Zheng, Y. Zong, H. Zhang and Z. Liu, *Chem. Soc. Rev.*, 2018, **47**, 5919–5945.

15 L. Kong, C. Tang, H. J. Peng, J. Q. Huang and Q. Zhang, *SmartMat*, 2020, **1**, 1–35.

16 M. J. Park and J. S. Lee, *Adv. Electron. Mater.*, 2019, **5**, 1800411.

17 H. Li, Y. Ma and Y. Huang, *Mater. Horiz.*, 2021, **8**, 383–400.

18 Z. Y. Wang, W. K. Zhang, X. L. Li and L. Z. Gao, *J. Mater. Res.*, 2016, **31**, 1648–1664.

19 L. B. Dong, C. J. Xu, Y. Li, Z. H. Huang, F. Y. Kang, Q. H. Yang and X. Zhao, *J. Mater. Chem. A*, 2016, **4**, 4659–4685.

20 Y. Yang, *Nanoscale*, 2020, **12**, 3560–3573.

21 J. Liu, J. Wang, C. Xu, H. Jiang, C. Li, L. Zhang, J. Lin and Z. X. Shen, *Adv. Sci.*, 2018, **5**, 1700322.

22 W. Liu, M. S. Song, B. Kong and Y. Cui, *Adv. Mater.*, 2017, **29**, 1603436.

23 R. Z. Hou, G. S. Gund, K. Qi, P. Nakhanivej, H. F. Liu, F. Li, B. Y. Xia and H. S. Park, *Energy Storage Mater.*, 2019, **19**, 212–241.

24 Y. Han, Y. Z. Lu, S. H. Shen, Y. Zhong, S. Liu, X. H. Xia, Y. X. Tong and X. H. Lu, *Adv. Funct. Mater.*, 2019, **29**, 1806329.

25 K. Wang, Y. Huang, M. Y. Wang, M. Yu, Y. D. Zhu and J. S. Wu, *Carbon*, 2017, **125**, 375–383.

26 Q. Yu, B. Jiang, J. Hu, C. Y. Lao, Y. Gao, P. Li, Z. Liu, G. Suo, D. He, W. A. Wang and G. Yin, *Adv. Sci.*, 2018, **5**, 1800782.

27 L. Manjakkal, C. G. Nunez, W. T. Dang and R. Dahiya, *Nano Energy*, 2018, **51**, 604–612.

28 H. Yao, F. Zhang, G. W. Zhang, H. Y. Luo, L. Liu, M. H. Shen and Y. Y. Yang, *Chem. Eng. J.*, 2018, **334**, 2547–2557.

29 J. Lee, J. Y. Seok, S. Son, M. Yang and B. Kang, *J. Mater. Chem. A*, 2017, **5**, 24585–24593.

30 C. Y. Wang, Z. J. Zheng, Y. Q. Feng, H. Ye, F. F. Cao and Z. P. Guo, *Nano Energy*, 2020, **74**, 104817.

31 C. W. Li, Q. C. Zhang, J. Sun, T. T. Li, E. Songfeng, Z. Z. Zhu, B. He, Z. Y. Zhou, Q. L. Li and Y. G. Yao, *ACS Energy Lett.*, 2018, **3**, 2761–2768.

32 Y. H. Wang, J. R. Zeng, J. Li, X. Q. Cui, A. M. Al-Enizi, L. J. Zhang and G. F. Zheng, *J. Mater. Chem. A*, 2015, **3**, 16382–16392.

33 B. Yuan and L. Cademartiri, *J. Mater. Sci. Technol.*, 2015, **31**, 607–615.

34 X. Wang, Z. Li, J. Shi and Y. Yu, *Chem. Rev.*, 2014, **114**, 9346–9384.

35 J. B. Wu, Z. W. Zhu, H. W. Zhang, H. M. Fu, H. Li, A. M. Wang and H. F. Zhang, *Sci. Rep.*, 2016, **6**, 1–7.
36 L. Wang, G. R. Yang, S. J. Peng, J. N. Wang, W. Yan and S. Ramakrishna, *Energy Storage Mater.*, 2020, **25**, 443–476.
37 J. N. Coleman, U. Khan, W. J. Blau and Y. K. Gun'ko, *Carbon*, 2006, **44**, 1624–1652.
38 Y. Liu and S. Kumar, *ACS Appl. Mater. Interfaces*, 2014, **6**, 6069–6087.
39 E. Z. Zhou, J. B. Xi, Y. Guo, Y. J. Liu, Z. Xu, L. Peng, W. W. Gao, J. Ying, Z. C. Chen and C. Gao, *Carbon*, 2018, **133**, 316–322.
40 B. Shi, Y. Shang, Y. Pei, S. Pei, L. Wang, D. Heider, Y. Y. Zhao, C. Zheng, B. Yang, S. Yarlagadda, T. W. Chou and K. K. Fu, *Nano Lett.*, 2020, **20**, 5504–5512.
41 Y. Yao, R. Xu, M. L. Chen, X. L. Cheng, S. F. Zeng, D. J. Li, X. F. Zhou, X. J. Wu and Y. Yu, *ACS Nano*, 2019, **13**, 4695–4704.
42 D. Gueon, J. T. Hwang, S. B. Yang, E. Cho, K. Sohn, D. K. Yang and J. H. Moon, *ACS Nano*, 2018, **12**, 226–233.
43 X. He, Y. Hu, R. Z. Chen, Z. Shen, K. S. Wu, Z. L. Cheng and P. Pan, *Chem. Eng. J.*, 2019, **360**, 1020–1029.
44 D. Li, L. Dai, X. Ren, F. Ji, Q. Sun, Y. Zhang and L. Ci, *Energy Environ. Sci.*, 2021, **14**, 424–436.
45 Y. X. Hu, D. L. Ye, B. Luo, H. Hu, X. B. Zhu, S. C. Wang, L. L. Li, S. J. Peng and L. Z. Wang, *Adv. Mater.*, 2018, **30**, 1703824.
46 H. Isobe, T. Tanaka, R. Maeda, E. Noiri, N. Solin, M. Yudasaka, S. Iijima and E. Nakamura, *Angew. Chem., Int. Ed.*, 2006, **45**, 6676–6680.
47 B. Koh and W. Cheng, *Langmuir*, 2014, **30**, 10899–10909.
48 Y. H. Zhu, X. Y. Yang, T. Liu and X. B. Zhang, *Adv. Mater.*, 2020, **32**, e1901961.
49 L. Ye, Y. Hong, M. Liao, B. J. Wang, D. C. Wei, H. S. Peng, L. Ye, Y. Hong, M. Liao, B. Wang, D. Wei and H. Peng, *Energy Storage Mater.*, 2020, **28**, 364–374.
50 Y. C. Li, J. W. Zhou, T. B. Zhang, T. S. Wang, X. L. Li, Y. F. Jia, J. L. Cheng, Q. Guan, E. Z. Liu, H. S. Peng and B. Wang, *Adv. Funct. Mater.*, 2019, **29**, 1808117.
51 M. Tehrani, *Phys. Status Solidi A*, 2021, **218**, 2000704.
52 B. Xu, H. R. Wang, Q. Z. Zhu, N. Sun, B. Anasori, L. F. Hu, F. Wang, Y. B. Guan and Y. Gogotsi, *Energy Storage Mater.*, 2018, **12**, 128–136.
53 Y. He, W. Chen, C. Gao, J. Zhou, X. Li and E. Xie, *Nanoscale*, 2013, **5**, 8799–8820.
54 Y. Shao, M. F. El-Kady, L. J. Wang, Q. Zhang, Y. Li, H. Wang, M. F. Mousavi and R. B. Kaner, *Chem. Soc. Rev.*, 2015, **44**, 3639–3665.
55 C. Hwang, W. J. Song, J. G. Han, S. Bae, G. Song, N. S. Choi, S. Park and H. K. Song, *Adv. Mater.*, 2018, **30**, 1705445.
56 D. Akinwande, N. Petrone and J. Hone, *Nat. Commun.*, 2014, **5**, 5678.
57 X. Y. Chia and M. Pumera, *Nat. Catal.*, 2018, **1**, 909–921.
58 P. Xiong, L. L. Peng, D. H. Chen, Y. Zhao, X. Wang and G. H. Yu, *Nano Energy*, 2015, **12**, 816–823.
59 P. Y. Chen, M. Liu, Z. Wang, R. H. Hurt and I. Y. Wong, *Adv. Mater.*, 2017, **29**, 1605096.
60 J. W. Ju, J. Ma, Y. T. Wang, Y. Y. Cui, P. X. Han and G. L. Cui, *Energy Storage Mater.*, 2019, **20**, 269–290.
61 L. L. Peng, Y. Zhu, D. H. Chen, R. S. Ruoff and G. H. Yu, *Adv. Energy Mater.*, 2016, **6**, 1600025.
62 E. Pomerantseva and Y. Gogotsi, *Nat. Energy*, 2017, **2**, 17089.
63 B. Mendoza-Sanchez and Y. Gogotsi, *Adv. Mater.*, 2016, **28**, 6104–6135.
64 K. S. Novoselov, V. I. Fal'ko, L. Colombo, P. R. Gellert, M. G. Schwab and K. Kim, *Nature*, 2012, **490**, 192–200.
65 Z. Qin, M. Taylor, M. Hwang, K. Bertoldi and M. J. Buehler, *Nano Lett.*, 2014, **14**, 6520–6525.
66 R. Van Noorden, *Nature*, 2012, **483**, S32–S33.
67 M. Lotya, P. J. King, U. Khan, S. De and J. N. Coleman, *ACS Nano*, 2010, **4**, 3155–3162.
68 S. Bae, H. Kim, Y. Lee, X. Xu, J. S. Park, Y. Zheng, J. Balakrishnan, T. Lei, H. R. Kim, Y. I. Song, Y. J. Kim, K. S. Kim, B. Ozyilmaz, J. H. Ahn, B. H. Hong and S. Iijima, *Nat. Nanotechnol.*, 2010, **5**, 574–578.
69 Y. Lee, S. Bae, H. Jang, S. Jang, S. E. Zhu, S. H. Sim, Y. I. Song, B. H. Hong and J. H. Ahn, *Nano Lett.*, 2010, **10**, 490–493.
70 K. P. Loh, Q. Bao, G. Eda and M. Chhowalla, *Nat. Chem.*, 2010, **2**, 1015–1024.
71 V. Chabot, D. Higgins, A. P. Yu, X. C. Xiao, Z. W. Chen and J. J. Zhang, *Energy Environ. Sci.*, 2014, **7**, 1564–1596.
72 V. Agarwal and P. B. Zetterlund, *Chem. Eng. J.*, 2021, **405**, 127018.
73 S. Thakur and N. Karak, *Carbon*, 2015, **94**, 224–242.
74 T. Hoshide, Y. Zheng, J. Hou, Z. Wang, Q. Li, Z. Zhao, R. Ma, T. Sasaki and F. Geng, *Nano Lett.*, 2017, **17**, 3543–3549.
75 P. Xiao, F. Bu, G. Yang, Y. Zhang and Y. Xu, *Adv. Mater.*, 2017, **29**, 1703324.
76 R. Huang, M. Huang, X. Li, F. An, N. Koratkar and Z. Z. Yu, *Adv. Mater.*, 2018, **30**, e1707025.
77 Z. Ling, C. E. Ren, M. Q. Zhao, J. Yang, J. M. Giammarco, J. Qiu, M. W. Barsoum and Y. Gogotsi, *Proc. Natl. Acad. Sci. U. S. A.*, 2014, **111**, 16676–16681.
78 A. Lipatov, H. Lu, M. Alhabeb, B. Anasori, A. Gruverman, Y. Gogotsi and A. Sinitskii, *Sci. Adv.*, 2018, **4**, eaat0491.
79 M. Q. Zhao, C. E. Ren, Z. Ling, M. R. Lukatskaya, C. Zhang, K. L. Van Aken, M. W. Barsoum and Y. Gogotsi, *Adv. Mater.*, 2015, **27**, 339–345.
80 Z. W. Zhang, H. N. Li, G. D. Zou, C. Fernandez, B. Z. Liu, Q. R. Zhang, J. Hu and Q. M. Peng, *ACS Sustainable Chem. Eng.*, 2016, **4**, 6763–6771.
81 M. O. Faruk, A. Ahmed, B. Adak, M. Marzana, M. M. Hossain and S. Mukhopadhyay, *J. Mater. Chem. C*, 2021, **9**, 10193–10215.
82 K. Liu, Y. Fan, A. Ali and P. K. Shen, *Nanoscale*, 2021, **13**, 2963–2971.
83 J. Zhou, M. Xie, F. Wu, Y. Mei, Y. Hao, L. Li and R. Chen, *Adv. Mater.*, 2022, **34**, 2106897.
84 H. Zhang, W. Q. Zhao, M. C. Zou, Y. S. Wang, Y. J. Chen, L. Xu, H. S. Wu and A. Y. Cao, *Adv. Energy Mater.*, 2018, **8**, 1800013.
85 X. Wang, K. Chen, G. Wang, X. Liu and H. Wang, *ACS Nano*, 2017, **11**, 11602–11616.

86 M. Govindasamy, S. Shanthi, E. Elaiyappillai, S. F. Wang, P. M. Johnson, H. Ikeda, Y. Hayakawa, S. Ponnusamy and C. Muthamizhchelvan, *Electrochim. Acta*, 2019, **293**, 328–337.
87 X. G. Gao, Y. Huang, Z. X. Guang and X. Li, *Energy Fuels*, 2020, **34**, 3931–3940.
88 Q. T. Zhou, J. N. Kim, K. W. Han, S. W. Oh, S. Umrao, E. J. Chae and I. K. Oh, *Nano Energy*, 2019, **59**, 120–128.
89 Z. Guo, H. Nie, Z. Yang, W. Hua, C. Ruan, D. Chan, M. Ge, X. Chen and S. Huang, *Adv. Sci.*, 2018, **5**, 1800026.
90 J. Ren, R. P. Ren and Y. K. Lv, *Chem. Eng. J.*, 2018, **353**, 419–424.
91 T. Chen, Y. A. Wang, Y. Yang, F. Huang, M. K. Zhu, B. T. W. Ang and J. M. Xue, *Adv. Funct. Mater.*, 2021, **31**, 2101607.
92 K. Wu, L. Zhang, Y. Yuan, L. Zhong, Z. Chen, X. Chi, H. Lu, Z. Chen, R. Zou, T. Li, C. Jiang, Y. Chen, X. Peng and J. Lu, *Adv. Mater.*, 2020, **32**, e2002292.
93 G. Y. Qian, X. B. Liao, Y. X. Zhu, F. Pan, X. Chen and Y. Yang, *ACS Energy Lett.*, 2019, **4**, 690–701.
94 T. Liu, M. Zhang, Y. L. Wang, Q. Y. Wang, C. Lv, K. X. Liu, S. Suresh, Y. H. Yin, Y. Y. Hu, Y. S. Li, X. B. Liu, S. W. Zhong, B. Y. Xia and Z. P. Wu, *Adv. Energy Mater.*, 2018, **8**, 1802349.
95 F. Wu, X. Gao, X. Xu, Y. Jiang, X. Gao, R. Yin, W. Shi, W. Liu, G. Lu and X. Cao, *ChemSusChem*, 2020, **13**, 1537–1545.
96 T. Zhang, L. Zhang, L. Zhao, X. Huang, W. Li, T. Li, T. Shen, S. Sun and Y. Hou, *Small*, 2020, **16**, e2005302.
97 C. Chen, S. Xu, Y. Kuang, W. Gan, J. Song, G. Chen, G. Pastel, B. Liu, Y. Li, H. Huang and L. Hu, *Adv. Energy Mater.*, 2019, **9**, 1802964.
98 J. H. Li, Y. L. Shao, Q. W. Shi, C. Y. Hou, Q. H. Zhang, Y. G. Li, R. B. Kaner and H. Z. Wang, *Nano Energy*, 2017, **38**, 429–437.
99 Z. Luo, C. Liu and S. Fan, *ACS Appl. Mater. Interfaces*, 2019, **11**, 42172–42178.
100 C. M. Shi, T. Y. Wang, X. B. Liao, B. Y. Qie, P. F. Yang, M. J. Chen, X. Wang, A. Srinivasan, Q. Cheng, Q. Ye, A. C. Li, X. Chen and Y. Yang, *Energy Storage Mater.*, 2019, **17**, 136–142.
101 G. Qian, B. Zhu, X. Liao, H. Zhai, A. Srinivasan, N. J. Fritz, Q. Cheng, M. Ning, B. Qie, Y. Li, S. Yuan, J. Zhu, X. Chen and Y. Yang, *Adv. Mater.*, 2018, **30**, e1704947.
102 A. Chen, X. Guo, S. Yang, G. J. Liang, Q. Li, Z. Chen, Z. D. Huang, Q. Yang, C. P. Han and C. Y. Zhi, *Energy Environ. Sci.*, 2021, **14**, 3599–3608.
103 X. B. Liao, C. M. Shi, T. Y. Wang, B. Y. Qie, Y. L. Chen, P. F. Yang, Q. Cheng, H. W. Zhai, M. J. Chen, X. Wang, X. Chen and Y. Yang, *Adv. Energy Mater.*, 2019, **9**, 1802998.
104 N. Nitta, F. X. Wu, J. T. Lee and G. Yushin, *Mater. Today*, 2015, **18**, 252–264.
105 K. Amin, Q. Meng, A. Ahmad, M. Cheng, M. Zhang, L. Mao, K. Lu and Z. Wei, *Adv. Mater.*, 2018, **30**, 1703868.
106 J. M. Son, S. Oh, S. H. Bae, S. Nam and I. K. Oh, *Adv. Energy Mater.*, 2019, **9**, 1900477.
107 S. R. Chen, R. M. Tao, J. Tu, P. M. Guo, G. Yang, W. J. Wang, J. Y. Liang and S. Y. Lu, *Adv. Funct. Mater.*, 2021, **31**, 2101199.
108 G. H. Chen, F. Zhang, Z. M. Zhou, J. R. Li and Y. B. Tang, *Adv. Energy Mater.*, 2018, **8**, 1801219.
109 S. Oh, V. H. Nguyen, V. T. Bui, S. Nam, M. Mahato and I. K. Oh, *ACS Appl. Mater. Interfaces*, 2020, **12**, 11657–11668.
110 D. Wei, W. Shen, T. Xu, K. Li, L. Yang, Y. Zhou, M. Zhong, F. Yang, X. Xu, Y. Wang, M. Zheng, Y. Zhang, Q. Li, Z. Yong, H. Li and Q. Wang, *Mater. Today Energy*, 2022, **23**, 100889.
111 Y. Gao, H. Hu, J. Chang, Q. Y. Huang, Q. N. Zhuang, P. Li and Z. J. Zheng, *Adv. Energy Mater.*, 2021, **11**, 2101809.
112 J. L. Xu, Y. H. Liu, X. Gao, S. Shen and S. D. Wang, *Energy Storage Mater.*, 2019, **22**, 402–409.
113 Y. Wang, X. Wang, X. Li, X. Li, Y. Liu, Y. Bai, H. Xiao and G. Yuan, *Adv. Funct. Mater.*, 2021, **31**, 2008185.
114 L. Kumar, P. K. Boruah, M. R. Das and S. Deka, *ACS Appl. Mater. Interfaces*, 2019, **11**, 37665–37674.
115 N. R. Chodankar, S. Selvaraj, S. H. Ji, Y. Kwon and D. H. Kim, *Small*, 2019, **15**, 1803716.
116 C. Chen, J. Cao, Q. Q. Lu, X. Y. Wang, L. Song, Z. Q. Niu and J. Chen, *Adv. Funct. Mater.*, 2017, **27**, 1604639.
117 H. Wu, Y. N. Zhang, W. Y. Yuan, Y. X. Zhao, S. H. Luo, X. W. Yuan, L. X. Zheng and L. F. Cheng, *J. Mater. Chem. A*, 2018, **6**, 16617–16626.
118 Q. Qin, J. Liu, W. Mao, C. Xu, B. Lan, Y. Wang, Y. Zhang, J. Yan and Y. Wu, *Nanoscale*, 2018, **10**, 7377–7381.
119 Y. H. Liu, J. L. Xu, X. Gao, Y. L. Sun, J. J. Lv, S. Shen, L. S. Chen and S. D. Wang, *Energy Environ. Sci.*, 2017, **10**, 2534–2543.
120 A. M. Bryan, L. M. Santino, Y. Lu, S. Acharya and J. M. D'Arcy, *Chem. Mater.*, 2016, **28**, 5989–5998.
121 J. Gamby, P. L. Taberna, P. Simon, J. F. Fauvarque and M. Chesneau, *J. Power Sources*, 2001, **101**, 109–116.
122 L. B. Dong, C. J. Xu, Q. Yang, J. Fang, Y. Li and F. Y. Kang, *J. Mater. Chem. A*, 2015, **3**, 4729–4737.
123 J. H. Jun, H. Song, C. Kim, I. S. Choi, Y. Jeong and J. H. Lee, *Small*, 2018, **14**, 1702145.
124 M. C. G. Santos, D. R. da Silva, P. S. Pinto, A. S. Ferlauto, R. G. Lacerda, W. P. Jesus, T. H. R. da Cunha, P. F. R. Ortega and R. L. Lavall, *Electrochim. Acta*, 2020, **349**, 136241.
125 L. B. Dong, G. M. Liang, C. J. Xu, D. Y. Ren, J. J. Wang, Z. Z. Pan, B. H. Li, F. Y. Kang and Q. H. Yang, *J. Mater. Chem. A*, 2017, **5**, 19934–19942.
126 F. H. Su and M. H. Miao, *Electrochim. Acta*, 2014, **127**, 433–438.
127 J. P. Li, S. Qiu, B. F. Liu, H. Y. Chen, D. S. Xiao and H. Li, *J. Power Sources*, 2021, **483**, 229219.
128 Q. Z. Liu, Z. H. Chen, S. S. Jing, H. Zhuo, Y. J. Hu, J. C. Liu, L. X. Zhong, X. W. Peng and C. F. Liu, *J. Mater. Chem. A*, 2018, **6**, 20338–20346.
129 Y. J. Li, W. Ou-Yang, X. T. Xu, M. Wang, S. J. Hou, T. Lu, Y. F. Yao and L. K. Pan, *Electrochim. Acta*, 2018, **271**, 591–598.
130 Y. Liu, J. Zhou, L. Chen, P. Zhang, W. Fu, H. Zhao, Y. Ma, X. Pan, Z. Zhang, W. Han and E. Xie, *ACS Appl. Mater. Interfaces*, 2015, **7**, 23515–23520.
131 Y. Y. Shen, Z. Y. Qin, S. Hu, L. F. Yang, X. Xu, L. Ding and Y. W. Zhang, *Carbon*, 2020, **158**, 711–718.

132 L. Huang, D. Santiago, P. Loyselle and L. Dai, *Small*, 2018, **14**, e1800879.

133 K. Lee, H. Lee, Y. Shin, Y. Yoon, D. Kim and H. Lee, *Nano Energy*, 2016, **26**, 746–754.

134 G. de Souza Augusto, J. Scarmínio, P. R. C. Silva, A. de Siervo, C. S. Rout, F. Rouxinol and R. V. Gelamo, *Electrochim. Acta*, 2018, **285**, 241–253.

135 C. J. Ye, Q. Q. Qin, J. Q. Liu, W. P. Mao, J. Yan, Y. Wang, J. W. Cui, Q. Zhang, L. P. Yang and Y. C. Wu, *J. Mater. Chem. A*, 2019, **7**, 4998–5008.

136 F. N. Dai, X. K. Wang, S. H. Zheng, J. P. Sun, Z. D. Huang, B. Xu, L. L. Fan, R. M. Wang, D. F. Sun and Z. S. Wu, *Chem. Eng. J.*, 2021, **413**, 127520.

137 Y. Yan, P. Gu, S. S. Zheng, M. B. Zheng, H. Pang and H. G. Xue, *J. Mater. Chem. A*, 2016, **4**, 19078–19085.

138 W. Zhao, Y. W. Zheng, L. Cui, D. D. Jia, D. Wei, R. K. Zheng, C. Barrow, W. R. Yang and J. Q. Liu, *Chem. Eng. J.*, 2019, **371**, 461–469.

139 S. Y. Zhou, X. Y. Kong, B. Zheng, F. W. Huo, M. Stromme and C. Xu, *ACS Nano*, 2019, **13**, 9578–9586.

140 Y. Yang, S. W. Ng, D. Chen, J. Chang, D. Wang, J. Shang, Q. Huang, Y. Deng and Z. Zheng, *Small*, 2019, **15**, e1902071.

141 K. F. Blurton and A. F. Sammells, *J. Power Sources*, 1979, **4**, 263–279.

142 M. A. Rahman, X. J. Wang and C. E. Wen, *J. Electrochem. Soc.*, 2013, **160**, A1759–A1771.

143 J. S. Lee, S. T. Kim, R. Cao, N. S. Choi, M. Liu, K. T. Lee and J. Cho, *Adv. Energy Mater.*, 2011, **1**, 34–50.

144 Q. F. Liu, Z. F. Pan, E. D. Wang, L. An and G. Q. Sun, *Energy Storage Mater.*, 2020, **27**, 478–505.

145 L. Wang, J. Pan, Y. Zhang, X. Cheng, L. Liu and H. Peng, *Adv. Mater.*, 2018, **30**, 1704378.

146 J. Lai, Y. Xing, N. Chen, L. Li, F. Wu and R. Chen, *Angew. Chem., Int. Ed.*, 2020, **59**, 2974–2997.

147 X. Chi, M. Li, J. Di, P. Bai, L. Song, X. Wang, F. Li, S. Liang, J. Xu and J. Yu, *Nature*, 2021, **592**, 551–557.

148 Z. Y. Guo, J. L. Li, Y. Xia, C. Chen, F. M. Wang, A. G. Tamirat, Y. G. Wang, Y. Y. Xia, L. Wang and S. H. Feng, *J. Mater. Chem. A*, 2018, **6**, 6022–6032.

149 C. Tang, B. Wang, H. F. Wang and Q. Zhang, *Adv. Mater.*, 2017, **29**, 1703185.

150 H. F. Wang, C. Tang and Q. Zhang, *Adv. Funct. Mater.*, 2018, **28**, 1803329.

151 X. Y. Cai, L. F. Lai, J. Y. Lin and Z. X. Shen, *Mater. Horiz.*, 2017, **4**, 945–976.

152 Y. G. Zhang, Y. P. Deng, J. Y. Wang, Y. Jiang, G. L. Cui, L. L. Shui, A. P. Yu, X. Wang and Z. W. Chen, *Energy Storage Mater.*, 2021, **35**, 538–549.

153 L. Yang, L. Shi, D. Wang, Y. L. Lv and D. P. Cao, *Nano Energy*, 2018, **50**, 691–698.

154 W. Wang, M. Tang, Z. Zheng and S. Chen, *Adv. Energy Mater.*, 2019, **9**, 1803628.

155 T. Zhang, Y. Tang, S. Guo, X. Cao, A. Pan, G. Fang, J. Zhou and S. Liang, *Energy Environ. Sci.*, 2020, **13**, 4625–4665.

156 X. Shen, T. Sun, L. Yang, A. Krasnoslobodtsev, R. Sabirianov, M. Sealy, W.-N. Mei, Z. Wu and L. Tan, *Nat. Commun.*, 2021, **12**, 820.

157 A. Ponrouch, J. Bitenc, R. Dominko, N. Lindahl, P. Johansson and M. R. Palacin, *Energy Storage Mater.*, 2019, **20**, 253–262.

158 Y. Liang, H. Dong, D. Aurbach and Y. Yao, *Nat. Energy*, 2020, **5**, 646–656.

159 P. Canepa, G. Sai Gautam, D. C. Hannah, R. Malik, M. Liu, K. G. Gallagher, K. A. Persson and G. Ceder, *Chem. Rev.*, 2017, **117**, 4287–4341.

160 H. L. Ye and Y. G. Li, *Energy Fuels*, 2021, **35**, 7624–7636.

161 J. Xie and Q. Zhang, *Small*, 2019, **15**, e1805061.

162 S. L. Lu, M. Y. Wang, F. Guo, J. G. Tu, A. J. Lv, Y. F. Chen and S. Q. Jiao, *Chem. Eng. J.*, 2020, **389**, 124370.

163 P. P. Wang, Z. Chen, H. Wang, Z. Y. Ji, Y. P. Feng, J. Q. Wang, J. Liu, M. M. Hu, J. B. Fei, W. Gan and Y. Huang, *Energy Storage Mater.*, 2020, **25**, 426–435.

164 A. Ponrouch, C. Frontera, F. Barde and M. R. Palacin, *Nat. Mater.*, 2016, **15**, 169–172.

165 M. Wang, C. Jiang, S. Zhang, X. Song, Y. Tang and H. M. Cheng, *Nat. Chem.*, 2018, **10**, 667–672.

166 J. Hyoung, J. W. Heo and S. T. Hong, *J. Power Sources*, 2018, **390**, 127–133.

167 P. Wang, H. Wang, Z. Chen, J. Wu, J. Luo and Y. Huang, *Nano Res.*, 2021, **15**, 701–708.

168 X. Zou, Q. Lu, Y. Zhong, K. Liao, W. Zhou and Z. Shao, *Small*, 2018, **14**, e1801798.

169 D. Xie, M. Zhang, Y. Wu, L. Xiang and Y. Tang, *Adv. Funct. Mater.*, 2019, **30**, 1906770.

170 Z. X. Liu, Q. Yang, D. H. Wang, G. J. Liang, Y. H. Zhu, F. N. Mo, Z. D. Huang, X. L. Li, L. T. Ma, T. C. Tang, Z. G. Lu and C. Y. Zhi, *Adv. Energy Mater.*, 2019, **9**, 1902473.

171 H. F. Li, C. P. Han, Y. Huang, Y. Huang, M. S. Zhu, Z. X. Pei, Q. Xue, Z. F. Wang, Z. X. Liu, Z. J. Tang, Y. K. Wang, F. Y. Kang, B. H. Li and C. Y. Zhi, *Energy Environ. Sci.*, 2018, **11**, 941–951.

172 F. Baskoro, H. Q. Wong and H. J. Yen, *ACS Appl. Energy Mater.*, 2019, **2**, 3937–3971.

173 X. Y. Fan, J. Liu, Z. S. Song, X. P. Han, Y. D. Deng, C. Zhong and W. B. Hu, *Nano Energy*, 2019, **56**, 454–462.

174 V. Vallem, Y. Sargolzaeiaval, M. Ozturk, Y. C. Lai and M. D. Dickey, *Adv. Mater.*, 2021, **33**, e2004832.

175 Z. Wu, Y. Wang, X. Liu, C. Lv, Y. Li, D. Wei and Z. Liu, *Adv. Mater.*, 2019, **31**, e1800716.

176 Y. Zhang, Q. Wang, S. Bi, M. Yao, F. Wan and Z. Niu, *Nanoscale*, 2019, **11**, 17630–17636.

177 D. Lee, H. Lee, O. Gwon, O. Kwon, H. Y. Jeong, G. Kim and S. Y. Lee, *J. Mater. Chem. A*, 2019, **7**, 24231–24238.

178 B. Wang, J. Li, C. Hou, Q. Zhang, Y. Li and H. Wang, *ACS Appl. Mater. Interfaces*, 2020, **12**, 46005–46014.

179 H. Z. Liu, J. H. Li, X. N. Zhang, X. X. Liu, Y. Yan, F. J. Chen, G. H. Zhang and H. G. Duan, *Adv. Funct. Mater.*, 2021, **31**, 2106550.

180 K. D. Harris, A. L. Elias and H. J. Chung, *J. Mater. Sci.*, 2016, **51**, 2771–2805.

181 A. M. Gaikwad and A. C. Arias, *ACS Appl. Mater. Interfaces*, 2017, **9**, 6390–6400.

182 H. Wang, J. Fu, C. Wang, R. Zhang, Y. Li, Y. Yang, H. Li, Q. Sun and H. Li, *InfoMat*, 2021, **4**, e12241.

183 L. J. Mao, Q. H. Meng, A. Ahmad and Z. X. Wei, *Adv. Energy Mater.*, 2017, **7**, 1700535.

184 H. F. Li, Z. J. Tang, Z. X. Liu and C. Y. Zhi, *Joule*, 2019, **3**, 613–619.

185 S. H. Kim, N. Y. Kim, U. J. Choe, J. M. Kim, Y. G. Lee and S. Y. Lee, *Adv. Energy Mater.*, 2021, **11**, 2100531.

186 Y. Bao, G. Hong, Y. Chen, J. Chen, H. Chen, W. L. Song and D. Fang, *ACS Appl. Mater. Interfaces*, 2020, **12**, 780–788.

187 C. J. Xu, L. Weng, B. B. Chen, L. Ji, J. Q. Zhou, R. Cai and S. L. Lu, *J. Power Sources*, 2020, **446**, 227353.

188 N. Li, H. Chen, S. Yang, H. Yang, S. Jiao and W. L. Song, *Adv. Sci.*, 2021, **8**, e2101372.

189 Y. Mao, G. Li, Y. Guo, Z. Li, C. Liang, X. Peng and Z. Lin, *Nat. Commun.*, 2017, **8**, 14628.

190 R. Z. Chen, Y. Hu, Z. Shen, P. Pan, X. He, K. S. Wu, X. W. Zhang and Z. L. Cheng, *J. Mater. Chem. A*, 2017, **5**, 12914–12921.

191 A. Mahmood, Z. W. Yuan, X. Sui, M. A. Riaz, Z. X. Yu, C. Liu, J. S. Chen, C. Wang, S. L. Zhao, N. Mahmood, Z. X. Pei, L. Wei and Y. Chen, *Energy Storage Mater.*, 2021, **41**, 395–403.

192 W. G. Chong, Y. Xiao, J. Q. Huang, S. Yao, J. Cui, L. Qin, C. Gao and J. K. Kim, *Nanoscale*, 2018, **10**, 21132–21141.

193 Z. Wang, A. Malti, L. Ouyang, D. Tu, W. Tian, L. Wagberg and M. M. Hamedi, *Small*, 2018, **14**, e1803313.

194 S. Y. Zhao, Y. Y. Zuo, T. Liu, S. Zhai, Y. W. Dai, Z. J. Guo, Y. Wang, Q. J. He, L. C. Xia, C. Y. Zhi, J. Bae, K. L. Wang and M. Ni, *Adv. Energy Mater.*, 2021, **11**, 2101749.

195 C. Shu, J. Long, S. X. Dou and J. Wang, *Small*, 2019, **15**, e1804701.

196 Y. N. Zhang, H. L. Qin, M. Alfred, H. Z. Ke, Y. B. Cai, Q. Q. Wang, F. L. Huang, B. Liu, P. F. Lv and Q. F. Wei, *Energy Storage Mater.*, 2021, **42**, 88–96.

197 G. Zan, T. Wu, Z. Zhang, J. Li, J. Zhou, F. Zhu, H. Chen, M. Wen, X. Yang, X. Peng, J. Chen and Q. Wu, *Adv. Sci.*, 2022, **9**, 2103714.

198 J. H. Park, M. J. Kwak, C. Hwang, K. N. Kang, N. Liu, J. H. Jang and B. A. Grzybowski, *Adv. Mater.*, 2021, **33**, e2101726.

199 A. Sumboja, M. Lubke, Y. Wang, T. An, Y. Zong and Z. L. Liu, *Adv. Energy Mater.*, 2017, **7**, 1700927.